

Article

Discovery of 1-(4-(4-Amino-3-(4-(2-morpholinoethoxy)phenyl)-1H-pyrazolo[3,4-d] pyrimidin-1-yl)phenyl)-3-(5-(tert-butyl)isoxazol-3-yl)urea (CHMFL-FLT3-213) as a Highly Potent Type II FLT3 Kinase Inhibitor Capable of Overcoming a Variety of FLT3 Kinase Mutants in FLT3-ITD Positive AML

Aoli Wang, Xixiang Li, Cheng Chen, Hong Wu, Ziping Qi, Chen Hu, Kailin Yu, Jiaxin Wu, Juan Liu, Xiaochuan Liu, Zhenquan Hu, Wei Wang, Wenliang Wang, Wenchao Wang, Li Wang, Beilei Wang, Qingwang Liu, Lili Li, Jian Ge, Tao Ren, Shanchun Zhang, Ruixiang Xia, Jing Liu, and Qingsong Liu
J. Med. Chem., **Just Accepted Manuscript** • DOI: 10.1021/acs.jmedchem.7b00840 • Publication Date (Web): 28 Sep 2017

Downloaded from <http://pubs.acs.org> on September 28, 2017

Just Accepted

“Just Accepted” manuscripts have been peer-reviewed and accepted for publication. They are posted online prior to technical editing, formatting for publication and author proofing. The American Chemical Society provides “Just Accepted” as a free service to the research community to expedite the dissemination of scientific material as soon as possible after acceptance. “Just Accepted” manuscripts appear in full in PDF format accompanied by an HTML abstract. “Just Accepted” manuscripts have been fully peer reviewed, but should not be considered the official version of record. They are accessible to all readers and citable by the Digital Object Identifier (DOI®). “Just Accepted” is an optional service offered to authors. Therefore, the “Just Accepted” Web site may not include all articles that will be published in the journal. After a manuscript is technically edited and formatted, it will be removed from the “Just Accepted” Web site and published as an ASAP article. Note that technical editing may introduce minor changes to the manuscript text and/or graphics which could affect content, and all legal disclaimers and ethical guidelines that apply to the journal pertain. ACS cannot be held responsible for errors or consequences arising from the use of information contained in these “Just Accepted” manuscripts.

1
2
3
4
5
6
7
8
9
10
11
12
13
14
15
16
17
18
19
20
21
22
23
24
25
26
27
28
29
30
31
32
33
34
35
36
37
38
39
40
41
42
43
44
45
46
47
48
49
50
51
52
53
54
55
56
57
58
59
60



SCHOLARONE™
Manuscripts

1
2
3
4
5
6
7
8
9
10
11
12
13
14
15
16
17
18
19
20
21
22
23
24
25
26
27
28
29
30
31
32
33
34
35
36
37
38
39
40
41
42
43
44
45
46
47
48
49
50
51
52
53
54
55
56
57
58
59
60

Discovery of 1-(4-(4-Amino-3-(4-(2-morpholinoethoxy)phenyl)-1*H*-pyrazolo[3,4-*d*]pyrimidin-1-yl)phenyl)-3-(5-(*tert*-butyl)isoxazol-3-yl)urea (CHMFL-FLT3-213) as a Highly Potent Type II FLT3 Kinase Inhibitor Capable of Overcoming a Variety of FLT3 Kinase Mutants in FLT3-ITD Positive AML

Aoli Wang^{1,2,7}, *Xixiang Li*^{1,2,7}, *Cheng Chen*^{1,3,7}, *Hong Wu*^{1,2,7}, *Ziping Qi*^{1,2,7}, *Chen Hu*^{1,3,7},
Kailin Yu^{1,3}, *Jiixin Wu*^{1,3}, *Juan liu*⁴, *Xiaochuan Liu*^{1,2}, *Zhenquan Hu*^{1,2}, *Wei Wang*^{1,2},
Wenliang Wang^{1,3}, *Wenchao Wang*^{1,2}, *Li Wang*^{1,3}, *Beilei Wang*^{1,3}, *Qingwang Liu*⁴, *Lili Li*⁵, *Jian Ge*⁵, *Tao Ren*⁴, *Shanchun Zhang*⁶, *Ruixiang Xia*^{5*}, *Jing Liu*^{1,2*}, *Qingsong Liu*^{1,2,3,4*}

1. High Magnetic Field Laboratory, Chinese Academy of Sciences, Mailbox 1110, 350 Shushanhu Road, Hefei, Anhui 230031, P. R. China
2. CHMFL-HCMTC Target Therapy Joint Laboratory, 350 Shushanhu Road, Hefei Anhui 230031, P. R. China
3. University of Science and Technology of China, Hefei, Anhui 230036, P. R. China

- 1
2
3 4. Precision Targeted Therapy Discovery Center, Institute of Technology Innovation,
4
5 Hefei Institutes of Physical Science, Chinese Academy of Sciences, Hefei, Anhui
6
7 230088, P. R. China
8
9
- 10 5. Department of Hematology, the First Affiliated Hospital of Anhui Medical
11
12 University, Hefei, Anhui 230022, P. R. China
13
14
- 15 6. Hefei Cosource Medicine Technology Co. LTD., 358 Ganquan Road, Hefei, Anhui
16
17 230031, P. R. China
18
19
- 20 7. These authors contribute equally
21
22

23 **ABSTRACT**

24
25
26
27 FLT3-ITD mutant has been observed in about 30% of AML patients and extensively
28
29 studied as a drug discovery target. Based on our previous study that Ibrutinib (**9**)
30
31 exhibited selective and moderate inhibitory activity against FLT3-ITD positive AML
32
33 cells, through a structure-guided drug design approach, we have discovered a new type II
34
35 FLT3 kinase inhibitor, compound **14** (CHMFL-FLT3-213), which exhibited highly
36
37 potent inhibitory effects against FLT3-ITD mutant and associated oncogenic mutations
38
39 (including FLT3-D835Y/H/V, FLT3-ITD-D835Y/I/N/A/G/Del and FLT3-ITD-F691L).
40
41 In the cellular context **14** strongly affected FLT3-ITD mediated signaling pathways and
42
43 induced apoptosis by arresting cell cycle into G0/G1 phase. In the in vivo studies **14**
44
45 demonstrated an acceptable bioavailability (F=19%) and significantly suppressed the
46
47 tumor growth in MV4-11 cell inoculated xenograft model (15 mg/kg/d, TGI=97%)
48
49 without exhibiting obvious toxicity. Compound **14** might be a potential drug candidate
50
51 for FLT3-ITD positive AML.
52
53
54
55
56
57
58
59
60

INTRODUCTION

Acute myeloid leukemia (AML) is one of the most common and lethal malignancies among children and young adults. Epidemiologic studies show that AML accounts for at least 3% of all human cancers, causing over 250 thousand cancer-related deaths annually. Fms-like tyrosine receptor kinase 3 (FLT3) plays an important role in normal hematopoiesis and leukemogenesis and is expressed in most AML blasts.¹ Mutation in the *FLT3* gene is the most frequent genetic alteration in AML and is well known as an important driver mutation for the development of myeloid malignancies.²

The most prevalent FLT3 mutant is the internal tandem duplication alteration (FLT3-ITD)³. Other important mutations occur in the tyrosine kinase domain (TKD), typically at the activation loop (AL) residue D835.⁴ These mutations are present in approximately 30% of all AML patients and lead to a far worse prognosis. Therefore, targeting FLT3 kinase is one of the current major efforts to fight against AML.

Over the last decade, many agents have been investigated as FLT3 inhibitors and tested in clinical trials. Based on the binding modes, these inhibitors could be classified as type I or type II⁵ depending on whether the compound binds to the “DFG-in” active kinase conformation (type I) or the “DFG-out” inactive kinase conformation (type II).⁶ As shown in Figure 1, compounds **1** (Sunitinib)⁷, **2** (Gilteritinib)⁸, **3** (Crenolanib)⁹ and **4** (Midostaurin)¹⁰ are type I inhibitors and recently compound **4** received a breakthrough therapy designation from the FDA for newly diagnosed FLT3-ITD positive AML. Compounds **5** (Pexidartinib)¹¹, **6** (Ponatinib)¹², **7** (Quizartinib)¹³ and **8** (Sorafenib)¹⁴ are type II inhibitors bearing FLT3 kinase activity and currently they are at different stages of clinical evaluation for AML.

1
2
3
4
5
6
7
8
9
10
11
12
13
14
15
16
17
18
19
20
21
22
23
24
25
26
27
28
29
30
31
32
33
34
35
36
37
38
39
40
41
42
43
44
45
46
47
48
49
50
51
52
53
54
55
56
57
58
59
60

In our previous studies, we found that BTK kinase inhibitor **9** (Ibrutinib), which has been approved for the treatment of mantle cell lymphoma (MCL)¹⁵ and chronic lymphocytic leukemia (CLL)¹⁶, exhibited selective and moderate inhibitory activity against FLT3-ITD mutant positive AML.¹⁷ Based on this observation, we have discovered a potent and selective type I FLT3 kinase inhibitor **10** (CHMFL-FLT3-122) that displayed impressive in vitro and in vivo activities against FLT3-ITD positive AML.¹⁸ However, compound **10** could not overcome the secondary mutations in the FLT3 kinase domain, *e.g.* ITD-F691L, which is located at the “gatekeeper” position in FLT3 that is analogous to residues in other kinases that are hotspots for drug-resistance to tyrosine kinase inhibitors (TKIs).⁹ Therefore, we continue to explore this pharmacophore and medicinal chemistry efforts led to the discovery of a novel type II FLT3 kinase inhibitor compound **14** (CHMFL-FLT3-213), which displayed potent in vitro and in vivo activities against FLT3-ITD and a variety of mutants including gatekeeper FLT3-ITD-F691L, FLT3-ITD-D835Y as well as FLT3-D835Y/H/V mutants (Figure 2).

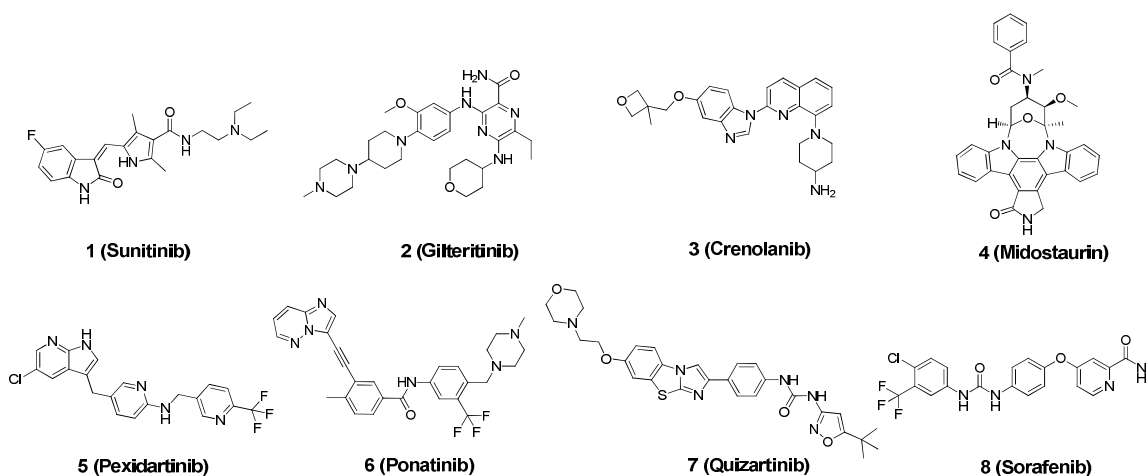


Figure 1. Chemical structures of representative FLT3 kinase inhibitors.

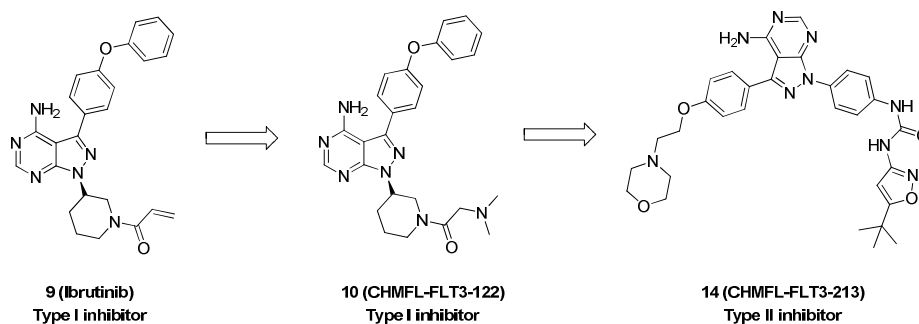


Figure 2. Schematic illustration of discovery of compound **14**.

RESULTS AND DISCUSSION

Design Rationale and Structure-Activity Relationship (SAR) Exploration

We first examined the binding mode of **9** with FLT3 kinase to understand the structural resistance mechanism. The result showed that the pyrazolopyrimidine core formed two hydrogen bonds with Cys694 and Glu692 respectively. The gatekeeper residue Phe691 positioned in parallel with the *O*-linked benzene ring which formed partial π - π interaction and strengthened the binding (Figure 3A). However, when Phe691 is mutated to leucine (F691L), the beneficial π - π interaction was lost and steric interaction between the benzene ring and leucine was introduced which weakened the binding (Figure 3B). This was confirmed by the observation that the antiproliferative efficacy (GI_{50}) of compound **9** significantly reduced from 0.12 μ M (BaF3-FLT3-ITD cell) to 2.5 μ M (BaF3-FLT3-ITD-F691L cell) (Table 1). In order to overcome this gatekeeper mutation induced drug resistance, such steric interaction should be avoided. This made us turn to the type II inhibitors because usually for type II inhibitors an amide or urea bond is required at this position to form the canonical hydrogen bonds with the amino acid residues located in the c-Helix and this would shift this moiety away from the

1
2
3 interaction with leucine (F691L). We also noticed that the pyrazolopyrimidine could form
4 the hinge binding if it was flipped 180 degree, although in this case it will only form two
5 hydrogen bonds with Cys694 but not with Cys694 and Glu692. Hence we reasoned that
6 introduction of proper type II binding elements at R₂ position (Table 1) would be able to
7 achieve the binding affinity.
8
9

10
11
12
13
14
15
16 Based on this postulation, we prepared compounds **11** and **12** which bear the urea
17 linkage at R₂ (Table 1). Further testing showed that **11** exhibited weak activity against
18 BaF3-FLT3-ITD cell (GI₅₀: 0.96 μM) and MV4-11 cell (GI₅₀: 0.65 μM). When changing
19 the cyclohexane ring to benzene ring for the connection of the amide (**12**), it gained
20 potent antiproliferative efficacy against BaF3-FLT3-ITD (GI₅₀: 0.001 μM). In addition, it
21 exhibited good selectivity over parental BaF3 cells (GI₅₀: >10 μM) and potent
22 antiproliferative effect against FLT3-ITD positive AML cells MV4-11 (GI₅₀: 0.021 μM).
23 Although compound **12** still could not overcome the FLT3-ITD-F691L mutation, its
24 potent inhibitory activity against FLT3-ITD indicated that type II binding might be
25 achieved and this encouraged us to study in detail of this new class of compounds.
26 Docking of **12** into the DFG-out inactive conformation of FLT3 kinase (PDB ID: 4XUF)
27 showed that the aminopyrimidine moiety formed two hydrogen bonds with Cys694 in the
28 hinge binding area (Figure 3C). As expected, the newly introduced urea linkage formed
29 two canonical hydrogen bonds with Glu661 in the cHelix and Asp829 in the DFG motif.
30 The *t*-butyl substituted isoxazole occupied the hydrophobic pocket generated by the
31 DFG-motif shift. In this binding mode, the diphenyl ether directed to the solvent exposed
32 area near the hinge binding area.
33
34
35
36
37
38
39
40
41
42
43
44
45
46
47
48
49
50
51
52
53
54
55
56
57
58
59
60

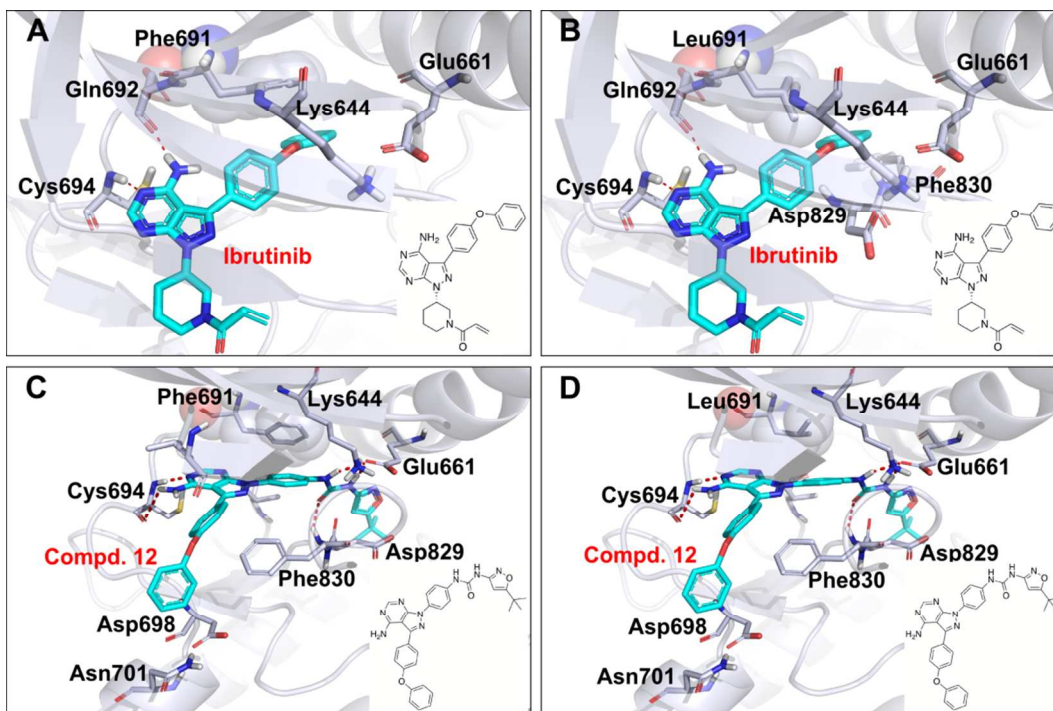


Figure 3. Design rationale of new FLT3 kinase inhibitor. (A) Docking of **9** into the active conformation of FLT3 wt kinase (homology model built from PDB ID: 4RT7 and 3LCD). (B) Docking of **9** into the active conformation of FLT3-F691L kinase (site mutation from FLT3 wt homology model). (C) Docking of **12** into the DFG-out inactive conformation of FLT3 wt kinase (PDB ID: 4XUF). (D) Docking of **12** into the active conformation of FLT3-F691L kinase (site mutation from PDB ID: 4XUF).

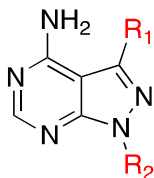
When the gatekeeper residue Phe691 is mutated to Leu691, the new leucine residue was away from the urea and should not be the hindrance for binding. However, the partial π - π interaction was lost and this could partially explain why compound **12** did not display inhibitory effect against FLT3-ITD-F691L mutant (Figure 3D). In addition, the polar environment formed by Asp698 and Asn701 surrounded the hydrophobic nonpolar diphenyl ether moiety in the hinge binding area, which may also disfavor this binding. Therefore, in order to further gain activity against FLT3-ITD-F691L, we removed one

1
2
3 benzene ring from the R₁ moiety (**13**, Table 1), which significantly improved its activity
4 to the mutant (GI₅₀: 0.11 μM for BaF3-FLT3-ITD-F691L cell). In addition, it also
5 increased the activity against FLT3-ITD (GI₅₀: <0.0003 μM for BaF3-FLT3-ITD cell and
6 GI₅₀: 0.001 μM for MV4-11 cell) meanwhile kept a good selectivity window to parental
7 BaF3 cell (GI₅₀: >10 μM). This result indicated that our postulation of binding analysis
8 was reasonable and we next further explored the SAR on the basis of this type II binding
9 mode.
10
11
12
13
14
15
16
17
18
19

20 Given the fact that R₁ moiety (Table 1) is exposed to the solvent area and more
21 hydrophilic group would be preferred, we then installed *O*-linked morpholine (**14**) into
22 compound **13**, which led to potent inhibition activity against FLT3-ITD (GI₅₀:
23 <0.0003 μM for BaF3-FLT3-ITD and MV4-11 cells) and FLT3-ITD-F691L (GI₅₀: 0.002
24 μM) meanwhile kept good selectivity over parental BaF3 cell (GI₅₀: >10 μM). Switching
25 the connection site of the benzene ring at R₁ from *-para* to *-meta* position (**15**) retained
26 the activity against FLT3-ITD but lost about 40-fold activity against FLT3-ITD-F691L.
27 Switching the connection site of the urea linkage at R₂ from *-para* to *-meta* position (**16**)
28 resulted in significant activity loss to both FLT3-ITD and F691L mutants. Interestingly,
29 changing the *tert*-butyl group at R₂ position that occupied the hydrophobic pocket
30 generated by the DFG motif shift to a methyl group (**17**) caused over 150-fold activity
31 loss against FLT3-ITD. Removal of the *tert*-butyl group (**18**) resulted in further activity
32 loss. Replacement of the isoxazole with thiazole (**19**) retained good inhibitory activity
33 against FLT3-ITD (GI₅₀: 0.021 μM) but lost activity to F691L mutant (GI₅₀: 5.6 μM).
34 Changing the *tert*-butyl group to a smaller CF₃ group (**20**) further decreased activity to
35 FLT3-ITD (GI₅₀: 0.17 μM) and completely lost activity to F691L mutant (GI₅₀: >10 μM).
36
37
38
39
40
41
42
43
44
45
46
47
48
49
50
51
52
53
54
55
56
57
58
59
60

1
2
3 Replacement of the *tert*-butyl isoxazole to *n*-butyl benzene (**21**) also retained good
4 activity against FLT3-ITD (GI₅₀: 0.024 μM) but lost activity to F691L mutant (GI₅₀: 8.7
5 μM). Increasing the hydrophobicity by installment of the 1-methyl-2-
6 (trifluoromethyl)benzene (**22**) enhanced activity to FLT3-ITD (GI₅₀: 0.002 μM) and
7 started to gain activity to F691L mutant (GI₅₀: 0.63 μM), although it was still much less
8 potent compared to **14**. A larger hydrophobic moiety 1,2,3-trimethoxybenzene (**23**) also
9 retained activity to FLT3-ITD (GI₅₀: 0.013 μM) but lost activity to F691L mutant (GI₅₀:
10 3.8 μM). Although introduction of a methyl group at the *-ortho* position of urea linkage
11 (**24**) retained activity to FLT3-ITD (GI₅₀: 0.046 μM) but not F691L mutant (GI₅₀: 1.4
12 μM), shifting the methyl group to *-meta* position (**25**) displayed good activity to both
13 FLT3-ITD (GI₅₀: 0.002 μM) and F691L mutants (GI₅₀: 0.013 μM). Elongation of the *O*-
14 linked morpholine with one more carbon at R₁ position (**26**) retained activity to FLT3-
15 ITD (GI₅₀: <0.0003 μM) but lost activity to F691L mutant (GI₅₀: 0.77 μM). Changing the
16 morpholine to piperidine (**27**) resulted in potent inhibition activity against FLT3-ITD
17 (GI₅₀: <0.0003 μM) and F691L mutants (GI₅₀: 0.023 μM). Installation of the hydrophilic
18 morpholine directly into the *-para* position of the benzene ring at R₁ position (**28**), or via
19 a carbonyl linkage (**29**), or a propionamide linkage (**30**) all retained potent activities to
20 FLT3-ITD but lost potency to F691L mutant. Attachment of hydrophilic groups such as
21 piperazine (**31**), methyl piperazine (**32**), ethyl piperazine (**33**), ethanol piperazine (**34**) and
22 ethyl piperidine (**35**) at R₁ position all resulted in high potencies against both FLT3-ITD
23 and F691L mutants, despite that they all displayed some activities against parental BaF3
24 cells (GI₅₀s: 1.0-3.3 μM). These results indicated that a polar hydrophilic group was
25 preferred to achieve both FLT3-ITD and gatekeeper F691L mutant activities.
26
27
28
29
30
31
32
33
34
35
36
37
38
39
40
41
42
43
44
45
46
47
48
49
50
51
52
53
54
55
56
57
58
59
60

Table 1. SAR Exploration at R₁/R₂ Positions by Examination of the Antiproliferation Efficacies against FLT3-ITD/F691L Transformed BaF3 and MV4-11 Cells^a



Compd.	R ₁	R ₂	BaF3-FLT3-ITD (GI ₅₀ : μM)	BaF3-FLT3-ITD-F691L (GI ₅₀ : μM)	Parental BaF3 (GI ₅₀ : μM)	MV4-11 (GI ₅₀ : μM)
9			0.12±0.005	2.5±0.1	>10	0.33±0.011
11			0.96±0.072	2.6±0.086	5.2±0.1	0.65±0.029
12			0.001±0.0003	7.9±0.056	>10	0.021±0.004
13			<0.0003	0.11±0.023	>10	0.001±0.0001
14			<0.0003	0.002±0.0009	>10	<0.0003
15			0.002±0.0001	0.082±0.005	>10	0.001±0.0005
16			0.87±0.032	4.6±0.28	6.9±0.1	0.56±0.04

17			0.056±0.008	>10	>10	0.069±0.007
18			0.24±0.015	5.4±0.15	>10	0.26±0.055
19			0.021±0.004	5.6±0.15	6.2±0.61	0.038±0.0068
20			0.17±0.03	>10	>10	0.26±0.015
21			0.024±0.001	8.7±0.21	>10	0.063±0.0006
22			0.002±0.0006	0.63±0.01	6.5±0.35	0.002±0.0006
23			0.013±0.002	3.8±0.11	>10	0.042±0.006
24			0.046±0.008	1.4±0.058	>10	0.12±0.005
25			0.002±0.0001	0.013±0.001	5.5±0.15	<0.0003
26			<0.0003	0.77±0.0067	6.4±0.28	0.001±0.0005
27			<0.0003	0.023±0.003	7.2±0.36	0.001±0.0005

28			<0.0003	0.16±0.005	>10	0.0014±0.0005
29			<0.0003	1.2±0.034	>10	0.002±0.0001
30			0.002±0.0001	0.17±0.011	>10	0.001±0.0005
31			<0.0003	0.008±0.001	2.8±0.15	<0.0003
32			<0.0003	0.10±0.006	3.3±0.11	<0.0003
33			<0.0003	0.013±0.003	1.9±0.058	<0.0003
34			<0.0003	0.008±0.0006	2.5±0.078	<0.0003
35			<0.0003	0.019±0.0025	1.0±0.072	<0.0003

^aAll GI₅₀ values were obtained by triplet testing (±SD).

Since compound **14** displayed best potencies against FLT3-ITD and FLT3-ITD-F691L gatekeeper mutants meanwhile exhibited best selectivity to parental BaF3 cells, we then further examined **14**'s activity against a panel of FLT3 mutants transformed BaF3 cells (Table 2). Not surprisingly, **14** displayed potent inhibitory activities against FLT3 wt, FLT3-ITD associated mutants including gatekeeper F691L,

D835Y/I/N/A/G/del as well as gain of function mutants including FLT3-D835Y/V/H. Compared to well-established type II FLT3 inhibitor **7**, **14** was more potent against FLT3-ITD-F691L/D835Y. Interestingly, neither **14** nor **7** were potent to FLT3-K663Q mutant.

Table 2. Antiproliferative Effects of Compounds **14** and **7** Against a Panel of FLT3 wt/mutants Transformed BaF3 Cells^a

Cell line	Compd. 14 (GI ₅₀ : μM)	Compd. 7 (GI ₅₀ : μM)
Parental BaF3	> 10	> 10
BaF3-TEL-FLT3 wt	<0.0003	<0.0003
BaF3-FLT3-ITD	<0.0003	<0.0003
BaF3-FLT3-ITD-F691L	0.002±0.0009	0.021±0.002
BaF3-FLT3-ITD-D835Y	0.002±0.0008	0.028±0.002
BaF3-FLT3-ITD-D835I	0.056±0.008	0.056±0.018
BaF3-FLT3-ITD-D835N	0.001±0.0005	<0.0003
BaF3-FLT3-ITD-D835G	<0.0003	<0.0003
BaF3-FLT3-ITD-D835A	0.0093±0.00006	<0.0003
BaF3-FLT3-ITD-D835del	0.046±0.0032	0.012±0.0015
BaF3-FLT3-D835Y	0.012±0.003	0.002±0.0001
BaF3-FLT3-D835V	0.003±0.0001	0.011±0.0005
BaF3-FLT3-D835H	<0.0003	<0.0003
BaF3-FLT3-K663Q	3.5±0.46	0.37±0.02

^aAll GI₅₀ values were obtained by triple testing (±SD).

Compound 14's Binding Mode

In order to better understand compound **14**'s binding mechanism, we then docked it into FLT3 wt X-ray structure (PDB ID: 4XUF)¹⁹ (Figure 4A). The modeling results showed that it adopted a typical type II binding mode with FLT3 kinase. The aminopyrimidine formed two hydrogen bonds with Cys694 in the hinge binding area. The urea moiety formed two signature type II binding hydrogen bonds with Gly661 in the cHelix and Asp829 in the DFG motif. The *tert*-butyl isoxazole occupied the hydrophobic pocket generated by the DFG motif shift. In addition, the morpholine moiety that directed into solvent exposed area formed a hydrogen bond with the Leu616 backbone carbonyl located in the P-loop after being protonated. This may explain why compound **14** was more potent than **12** which is because the latter compound lacks such hydrogen bond. In the F691L mutant model (site mutation from PDB ID: XUF) compound **14** adopted a similar type II binding mode (Figure 4B). In this binding model, three hydrogen bonds formed by the urea moiety turned the benzene ring away from this position, which generated enough space to accommodate the Leu691 residue. This may explain why compound **14** was still sensitive to the F691L mutant. The hydrogen bond between the nitrogen atom in the morpholine and Leu616 played critical roles for the binding because compounds like **31-35** that bore a similar nitrogen atom at this position all displayed potent inhibition activity to both FLT3-ITD and F691L mutants. However, compounds **28-30** which lack this hydrogen bond formation capability lost activities to F691L mutant. In addition, when a methyl group was introduced to the *-ortho* position of this benzene ring (**24**), a hindrance interaction between Leu691 or Asp829 disfavored the binding (Figure 4C). However, when the methyl group was introduced to the *-meta*

position, there was enough space to accommodate it, which explained why compound **25** was still potent to both FLT3-ITD and F691L mutants (Figure 4D). Comparably, compound **7** adopted a similar type II binding mode except for the hinge region, where the sulfur atom in the imidazobenzothiazole ring forms a weak hydrogen bond with the backbone nitrogen of Cys694. In addition, the weak π - π stacking interactions between Tyr693 in the hinge region and the imidazobenzothiazole ring also increased the binding affinity.¹⁹

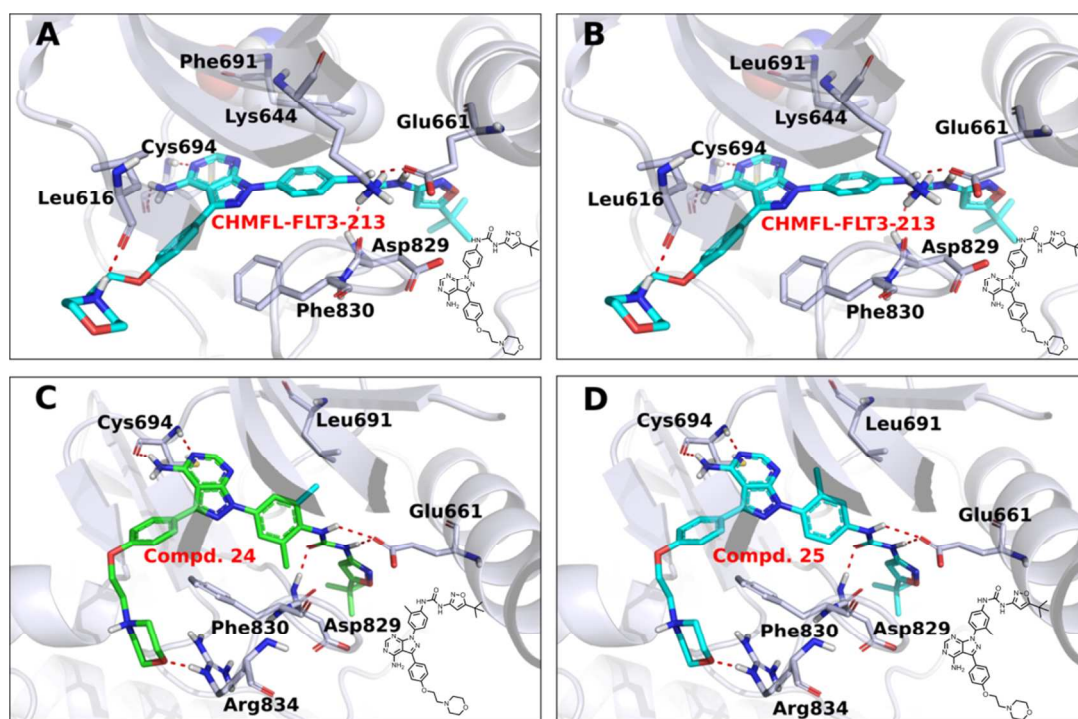


Figure 4. Binding mode examination of compound **14**. (A) Docking of **14** into the DFG-out conformation of FLT3 kinase (PDB ID: 4XUF). (B) Docking of **14** into the homology model of DFG-out conformation of FLT3-F691L mutant (site mutation from PDB ID: 4XUF). (C) Docking of **24** into the homology model of DFG-out conformation of FLT3-F691L mutant (Green and blue color represents two possible directions of methyl group

1
2
3 respectively). (D) Docking of **25** into the homology model of DFG-out conformation of
4
5
6 FLT3-F691L mutant.
7

8 9 **Compound 14's Selectivity Profiling**

10
11 In order to further understand compound **14**'s selectivity, we then examined its
12
13 kinome wide selectivity profile with KINOMEScan technology²⁰. The results showed
14
15 that **14** possessed a good selectivity (S score (1) = 0.04) in a panel of 468 kinases and
16
17 mutants at 1 μ M concentration (Figure 5A and supplemental Table 1). Not surprisingly,
18
19 **14** displayed strong binding affinities against FLT3 wt and FLT3 (ITD) as well as a
20
21 number of mutants including FLT3 D835H/K663Q/R834Q. In addition, it presented
22
23 strong binding activities to CDK11, CDK7, CDK8, CDKL2, CIT, CSF1R, DDR1,
24
25 DDR2, FLT4, KIT, LCK, LOK, MKNK2, PDGFRA, PDGFRB, and RET kinases
26
27 (percent activity remaining less than 1% at 1 μ M) (Figure 5B). Given the fact that
28
29 KINOMEScan is a binding assay and may not fully reflect the inhibitory activities, we
30
31 then used Invitrogen's Z'Lyte based and ADP-Glo based biochemical activity assays to
32
33 further confirm these potential targets (Figure 5C). The results demonstrated that **14**
34
35 inhibited FLT3 wt (IC₅₀: 91 nM), FLT3-ITD (IC₅₀: 9 nM), CDK11 (IC₅₀: 36 nM), CDK8
36
37 (IC₅₀: 48 nM), DDR1 (IC₅₀: 63 nM), DDR2 (IC₅₀: 61 nM), LCK (IC₅₀: 425 nM), FLT4
38
39 (IC₅₀: 141 nM), PDGFR α (IC₅₀: 426 nM), PDGFR β (IC₅₀: 606 nM), RET (IC₅₀: 32 nM),
40
41 KIT (IC₅₀: 83 nM) and CSF1R (IC₅₀: 154 nM) kinases, respectively. We also used ADP-
42
43 Glo based biochemical activity assays to test positive compound **7** and the results showed
44
45 that **7** inhibited FLT3 wt (IC₅₀: 30.4 nM) as well as FLT3-ITD (IC₅₀: 16.8 nM). Moreover,
46
47 **7**'s selectivity profile has been published¹³ and the results demonstrated that **7** also
48
49 showed strong binding constants against DDR1 (K_d: 81 nM), DDR2 (K_d: 690 nM),
50
51
52
53
54
55
56
57
58
59
60

1
2
3
4
5
6
7
8
9
10
11
12
13
14
15
16
17
18
19
20
21
22
23
24
25
26
27
28
29
30
31
32
33
34
35
36
37
38
39
40
41
42
43
44
45
46
47
48
49
50
51
52
53
54
55
56
57
58
59
60

FLT4 (Kd: 41 nM), PDGFR α (Kd: 11 nM), PDGFR β (Kd: 7.7 nM), RET (Kd: 9.9 nM), KIT (Kd: 4.8 nM), CSF1R (Kd: 12 nM) and FLT1 (Kd: 41 nM) kinases. We then used the TEL transformed BaF3 system to further confirm the on-target activity and selectivity against other potential off-targets revealed by KINOMEScan binding assay (Table 3). The data showed that **14** could potently inhibit PDGFR α (GI₅₀ <0.0003 μ M), PDGFR β (GI₅₀ <0.0003 μ M), KIT (GI₅₀ = 0.001 μ M) as well as RET (GI₅₀ = 0.04 μ M) kinase transformed BaF3 cells. This is not surprising because cKIT, FLT3 and PDGFR kinases all belong to the type III receptor tyrosine kinase family and the ATP binding pocket of these kinases are highly conserved. In addition, CSF1R, DDR1/2, FLT4 and LCK kinase transformed BaF3 cells were not potently inhibited which indicated that **14** might not really potently inhibit those kinases in cell. In comparison, compound **7** displayed more potent activities than compound **14** against CSF1R, DDR1, DDR2, FLT4 and LCK kinases. Both of them potently inhibited cKIT and PDGFR α/β kinases besides FLT3-ITD kinase. In addition, compound **14** was more potent against RET kinase than compound **7** (Table 3).

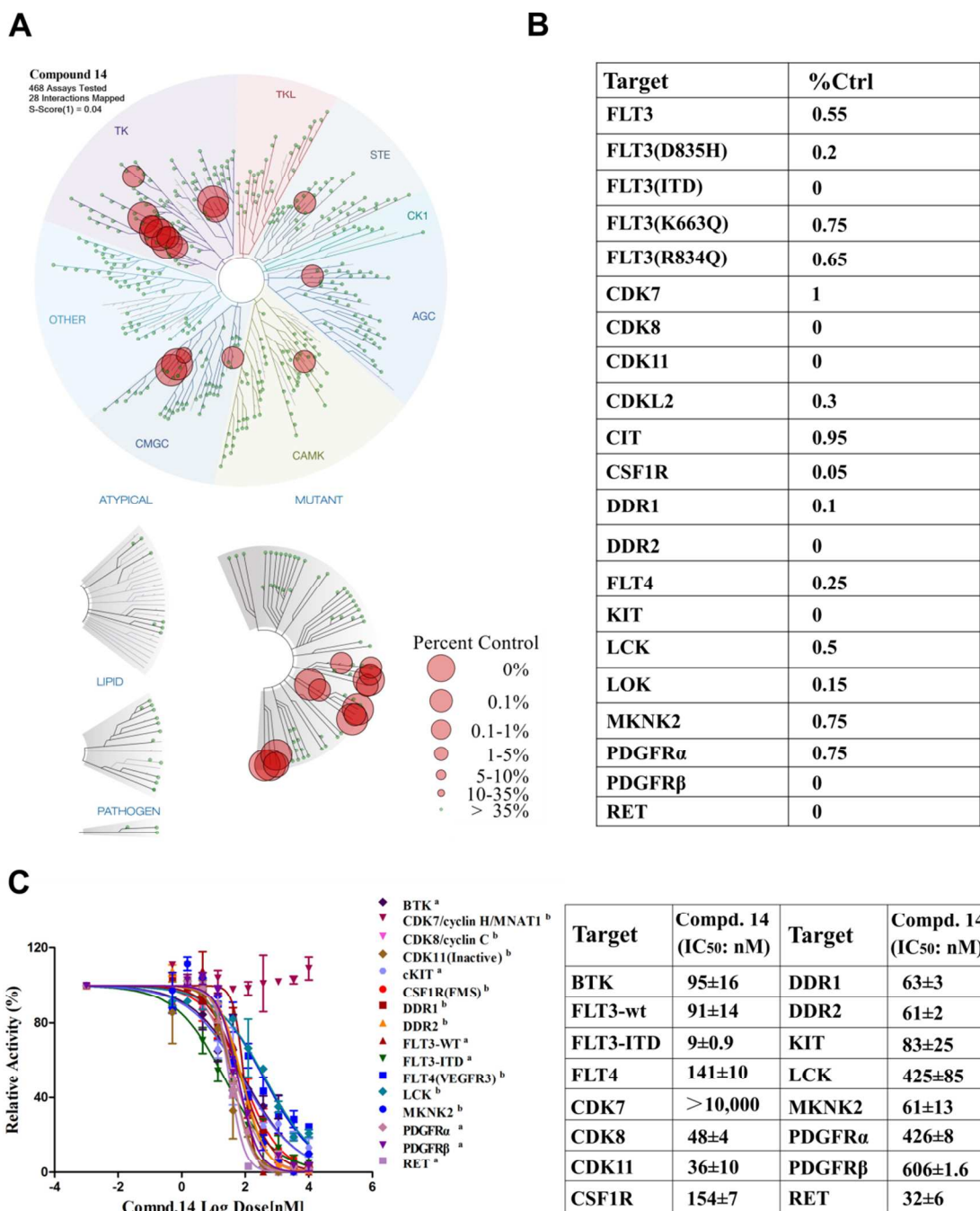


Figure 5. Kinome wide selectivity profiling of compound **14** with DiscoverX KINOMEScan technology. Measurements were performed at a concentration of 1 μ M of the inhibitor. The affinity was defined with respect to a DMSO control. (A) Treemap demonstration of **14**'s selectivity in 468 kinase targets. (B) Other targets that

demonstrated strong binding to **14** with a percent control number less than 1. (C) ADP-Glo assay and Invitrogen's biochemical characterization of **14**. (^aThe biochemical tests used ADP-Glo assay (Promega, Madison, WI). ^bThe biochemical tests were provided by Invitrogen (Carlsbad, CA, USA). All data was obtained by triplet testing (\pm SD).

Table 3. Antiproliferative Efficacy of Compounds **14** and **7** Against a Panel of Kinase Transformed BaF3 Cells^a

Cell line	Compd. 14 (GI ₅₀ : μ M)	Compd. 7 (GI ₅₀ : μ M)
Parental BaF3	> 10	> 10
BaF3-TEL-CSF1R	0.29 \pm 0.026	0.024 \pm 0.003
BaF3-TEL-DDR1	> 10	0.12 \pm 0.02
BaF3- TEL-DDR2	6.4 \pm 0.23	0.11 \pm 0.02
BaF3-TEL-FLT4	2.0 \pm 0.056	0.27 \pm 0.06
BaF3-TEL-cKIT	0.001 \pm 0.0007	0.017 \pm 0.001
BaF3-TEL-LCK	3.7 \pm 0.1	0.4 \pm 0.06
BaF3-TEL-PDGFR α	<0.0003	<0.0003
BaF3-TEL-PDGFR β	<0.0003	0.0044 \pm 0.0001
BaF3-TEL-RET	0.04 \pm 0.002	0.13 \pm 0.01

^aAll GI₅₀ values were obtained by triple testing (\pm SD).

Compound **14**'s In Cell Activity Evaluation

We next tested compound **14** against a panel of established AML cancer cell lines. The results showed that it could selectively and strongly inhibit the proliferation of FLT3-ITD positive AML cell lines such as MOLM13, MOLM14 and MV4-11 (GI₅₀S: <0.0003 μ M) meanwhile exhibited good selectivity over FLT3 wt expressing cell lines

such as U937 (GI_{50} : 4.2 μ M), SKM-1 (GI_{50} : 8.9 μ M), NB4 (GI_{50} : 5.4 μ M), OCI-AML-2 (GI_{50} : 8.5 μ M), HL-60 (GI_{50} : 1.1 μ M) as well as CMK (GI_{50} : 1.1 μ M). The well established type II FLT3 inhibitor compound **7** also displayed similar potencies against FLT3-ITD positive cell lines but for FLT3-wt expressing cell lines it bore narrower selectivity window compared to compound **14** (Table 4).

Table 4. Antiproliferative Effects of Compounds **14** and **7** Against a Panel of AML Cancer Cell Lines^a

Cell line	Compd. 14 (GI_{50} : μ M)	Compd. 7 (GI_{50} : μ M)
MOLM-13 (FLT3-ITD)	<0.0003	<0.0003
MOLM-14 (FLT3-ITD)	<0.0003	<0.0003
MV4-11 (FLT3-ITD)	<0.0003	<0.0003
U937 (FLT3-wt)	4.2 \pm 0.057	1.2 \pm 0.1
SKM-1 (FLT3-wt)	8.9 \pm 0.11	1.3 \pm 0.058
NB4 (FLT3-wt)	5.4 \pm 0.15	7.3 \pm 0.15
OCI-AML-2 (FLT3-wt)	8.5 \pm 0.11	>10
HL-60 (FLT3-wt)	1.1 \pm 0.057	0.13 \pm 0.035
CMK (FLT3-wt)	1.1 \pm 0.058	0.12 \pm 0.0056

^aAll GI_{50} values were obtained by triple testing (\pm SD).

We then examined compound **14**'s effects on the FLT3 mediated signaling pathways in MOLM-13, MOLM-14 and MV4-11 cells (Figure 6A). As the results demonstrated,

1
2
3 compound **14** completely blocked FLT3 auto-phosphorylation at Tyr589/591 site at the
4
5 concentration of 1 nM, and also remarkably inhibited the downstream signaling
6
7 mediators pSTAT5 (Tyr694), pERK (Thr202/Tyr204) and pAKT (Thr308/Ser473)(EC₅₀
8
9 less than 10 nM). In addition, the expression of c-Myc was also significantly down
10
11 regulated. Compound **14** could also effectively arrest cell cycle into the G₀/G₁ phase
12
13 starting from a concentration of 10 nM in these cells (Figure 6B). Furthermore, apparent
14
15 apoptosis was observed by examining the cleavage of PARP and caspase-3 proteins
16
17 (Figure 6C). Comparably, similar dose-responsive results were observed for positive
18
19 control compound **7** (Supplemental Figure 1).
20
21
22
23
24
25
26
27
28
29
30
31
32
33
34
35
36
37
38
39
40
41
42
43
44
45
46
47
48
49
50
51
52
53
54
55
56
57
58
59
60

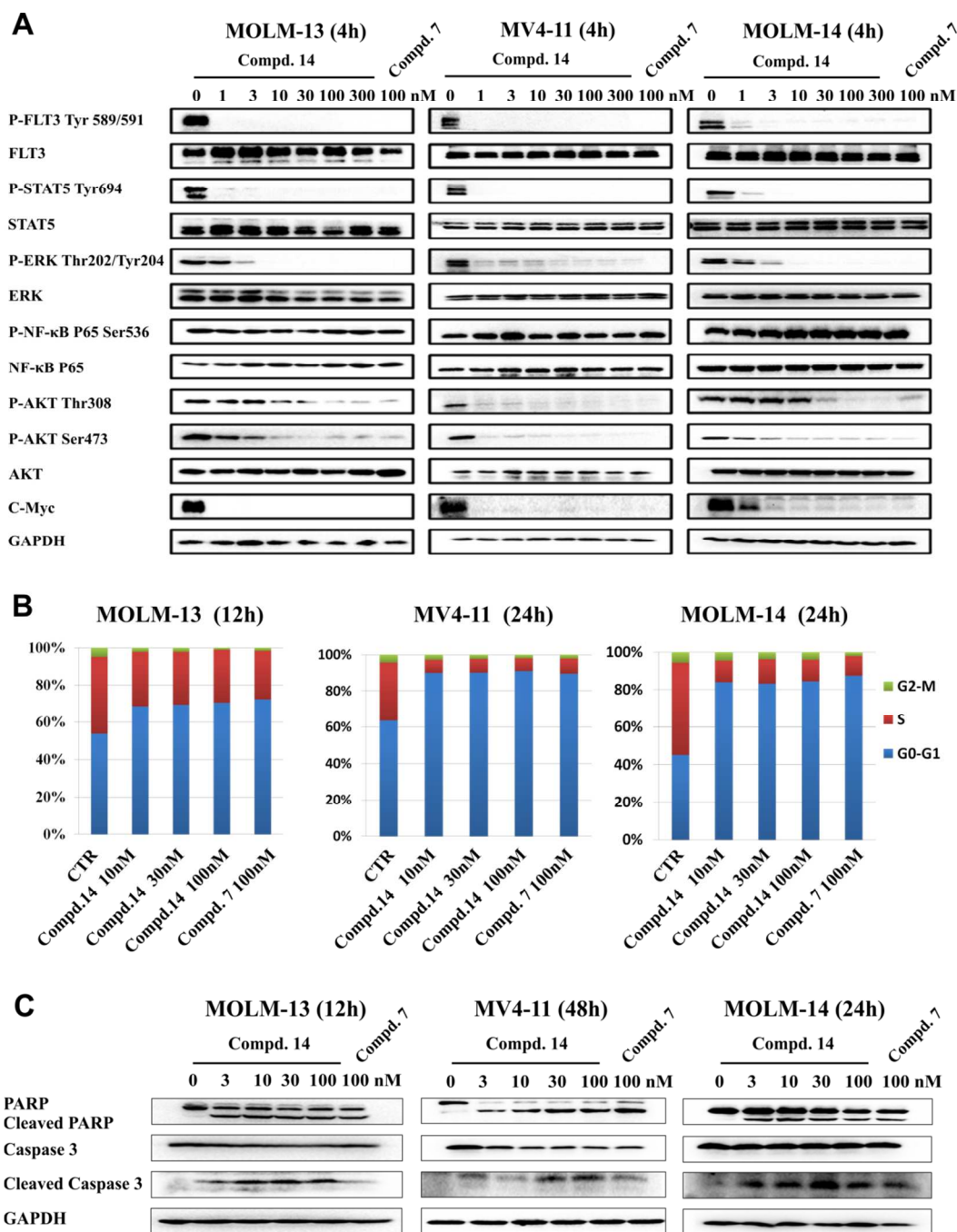


Figure 6. Cellular effects of compound **14** in FLT3-ITD positive AML cell lines. (A) Effects of **14** on FLT3 mediated signaling pathways. (B) Effects of **14** on cell cycle progression. (C) Effects of **14** on apoptosis. All data were obtained by duplicate runs and only one run was shown as representative.

In Vivo PK/PD Evaluation.

We next evaluated compound **14** and **7**'s PK properties in rats following intravenous and oral administration (Table 5). Upon oral administration it showed a half-life ($T_{1/2}$) of 3.61 h and a bioavailability (F) of 18.8 %, which indicated that **14** was suitable for oral application in the following animal efficacy study. In comparison, compound **7** exhibited much better PK profile than compound **14** regarding to the AUC, C_{max} and bioavailability.

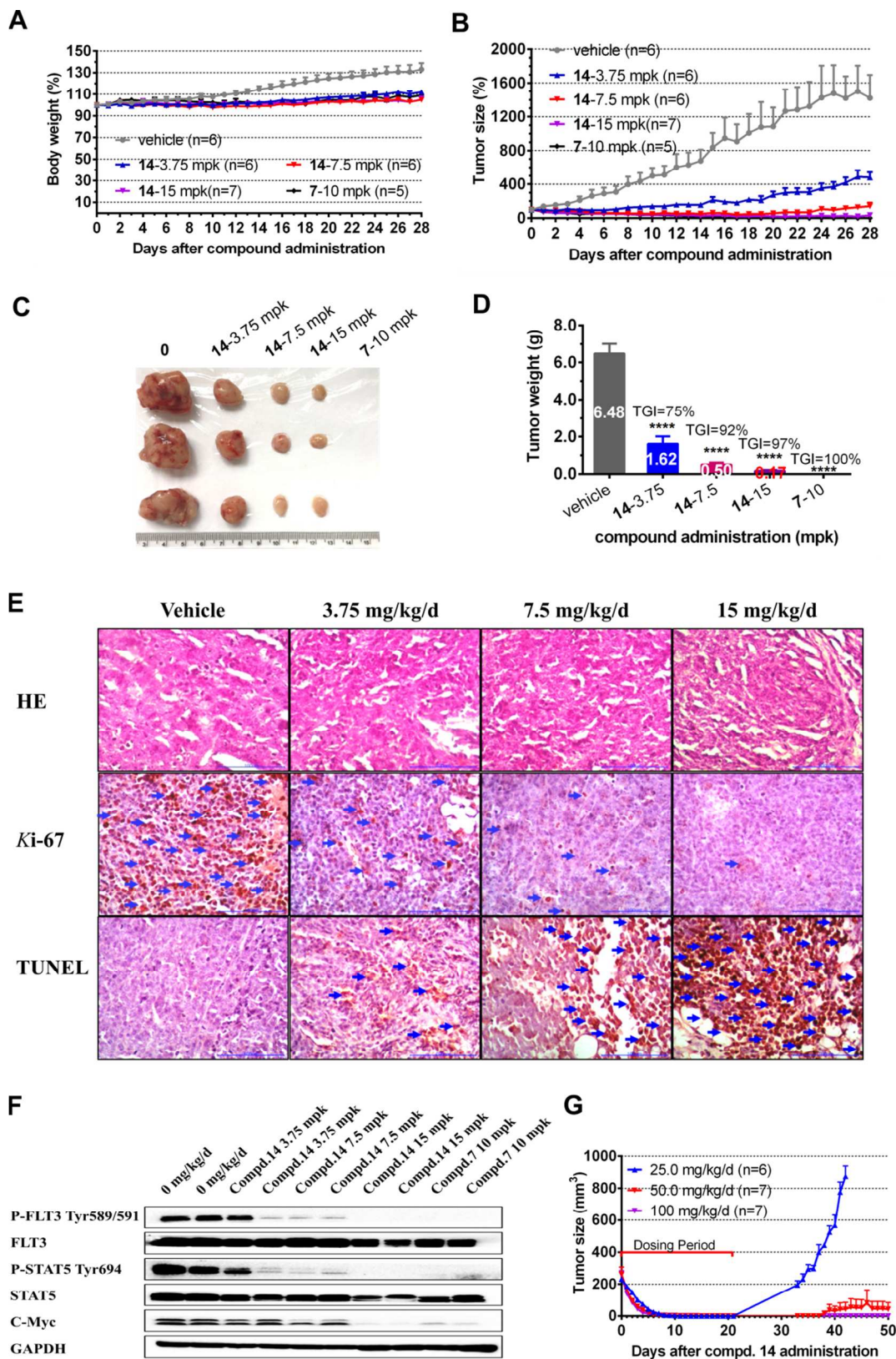
Table 5. Pharmacokinetic Study of Compounds **14** and **7** on Sprague Dawley Rats^a

Compd. 14	I.V. (1 mg/mg)	P.O. (10 mg/mg)	Compd. 7	I.V. (1 mg/mg)	P.O. (10 mg/mg)
AUC _(0-t) (ng/mL·h)	519.81±165.64	978.32±482.72	AUC _(0-t) (ng/mL·h)	1928±754	14467±6599
AUC _(0-∞) (ng/mL·h)	524.69±170.77	990.719±489.86	AUC _(0-∞) (ng/mL·h)	1973±785	14970±6980
C _{max} (ng/mL)	839.39±111.18	83.50±50.90	C _{max} (ng/mL)	728±117	1142±495
T _{max} (h)	0.017±0	6.66±1.15	T _{max} (h)	0.03±0	8.00±3.46
T _{1/2} (h)	3.34±1.22	3.61±0.46	T _{1/2} (h)	4.38±0.24	3.73±0.15
V _z (mL/kg)	9.09±0.72	60.82±26.87	V _z (mL/kg)	3532±1244	4078±1539
CL _z (mL/h/kg)	2.07±0.78	11.56±4.45	CL _z (mL/h/kg)	561±208	756±284
MRT _(0-∞) (h)	3.13±0.70	7.22±0.12	MRT _(0-∞) (h)	5.83±1.47	10.11±1.27
F (%)	/	18.8	F (%)	/	75.9

^aAll testing data were obtained from three independent mice. (±SD)

The antitumor efficacy of compound **14** was tested in MV4-11 cell (which bears exclusive FLT3-ITD mutation genes) inoculated xenograft mouse model. The results

1
2
3 demonstrated that dosages of 3.75, 7.5 and 15 mg/kg/day through oral administration did
4 not significantly affect the mice body weight (Figure 7A). During 28 days of continuous
5 treatment, **14** dose-dependently suppressed the MV4-11 tumor progression and a dosage
6 of 15 mg/kg/day exhibited the TGI (tumor growth inhibition) of 97% (Figure 7B-D).
7
8 However, compound **7** showed better activity at a dosage of 10 mg/kg/day with 100%
9 TGI, which reflected its superior PK profile than compound **14**. Immunohistochemistry
10 stain results demonstrated that **14** could dose dependently inhibit cancer cell proliferation
11 (*Ki-67* stain) and induce apoptosis (TUNEL stain) in the tumor tissues (Figure 7E). In
12 addition, immunoblotting analysis of the extracted tumor cells from the tumor tissues
13 after drug treatment showed that FLT3 mediated signaling pathways were potently
14 inhibited, which further confirmed that compound **14** exhibited its anti-tumor efficacy
15 through FLT3 on-target effect (Figure 7F). Since the clinically advanced FLT3 inhibitor
16 compound **7** is known to prevent the tumor regrowth upon stopping the treatment, we
17 also examined this trend for compound **14**. At 25 mg/kg/day, tumors appeared to regrow
18 after stop of **14** treatment. In contrast, the tumors only slightly regrow after day 38 (17
19 days post last dose) with 50 mg/kg dose of **14**. Moreover, the 100 mg/kg/day dose of **14**
20 completely inhibited tumor regrowth in the 50 days observation (Figure 7G).
21
22
23
24
25
26
27
28
29
30
31
32
33
34
35
36
37
38
39
40
41
42
43
44
45
46
47
48
49
50
51
52
53
54
55
56
57
58
59
60



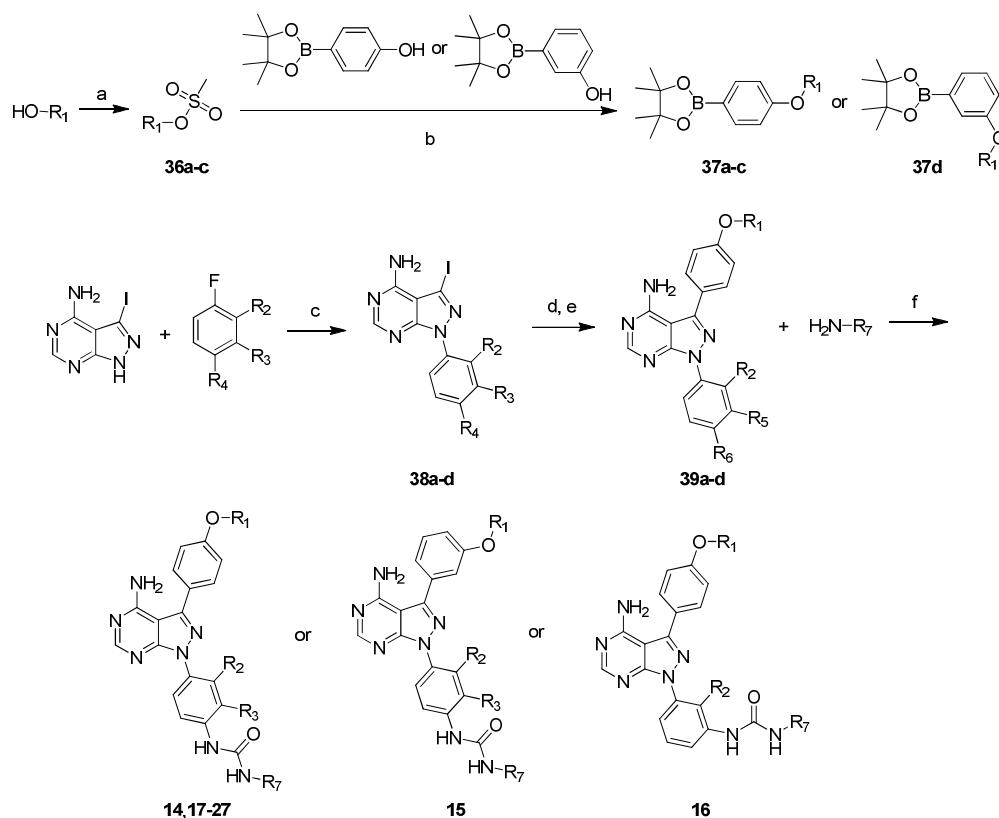
1
2
3 **Figure 7.** Compound **14**'s antitumor efficacy in MV4-11 cell (FLT3-ITD) inoculated
4 xenograft mouse model. Female nu/nu mice bearing established MV4-11 tumor
5 xenografts were treated with **14** at 3.75, 7.5 and 15 mg/kg/d dosage or **7** at 10 m/kg/d or
6 vehicle. Daily oral administration was initiated when MV4-11 tumors had reached a size
7 of 200 to 400 mm³. Each group contained 5-7 animals. Data, mean \pm SEM. mpk,
8 mg/kg/d. (A) Body weight and (B) Tumor size measurements from MV4-11 xenograft
9 mice after 28 days compound administration. Initial body weight and tumor size were set
10 as 100%. (C) Representative photographs of tumors in each group after 0, 3.75, 7.5 and
11 15 mg/kg/d **14** or 10 m/kg/d **7** treatments. (D) Comparison of the final tumor weights in
12 each group after 28-day treatment period. Numbers in columns indicate the mean tumor
13 weight in each group. (****) $p < 0.0001$. (E) Representative micrographs of hematoxylin
14 and eosin (HE), Ki-67 and TUNEL staining of tumor tissues with **14** treatment groups in
15 comparison with the vehicle treatment group. Note the specific nuclear staining of cells
16 with morphology consistent with proliferation and apoptosis (E, blue arrows). (F) Dose-
17 responsive immunoblotting of the signaling pathway with the cells extracted from tumor
18 tissues of the experimental animal after the **14** and **7** treatments. (G) Tumor progression
19 examination after stopping compound **14** treatment.

44 CHEMISTRY

45
46
47 Compounds **14-27** were prepared as shown in Scheme 1. The synthesis started from *O*-
48 esterification between R₁-substituted alcohol and methanesulfonyl chloride, which
49 generated intermediates **36a-c**. Then *O*-alkylation between **36a-c** and 4- or 3-(4,4,5,5-
50 tetramethyl-1,3,2-dioxaborolan-2-yl)phenol provided intermediates **37a-d**. Nucleophilic
51 substitution of 3-iodo-1*H*-pyrazolo[3,4-*d*]pyrimidin-4-amine with substituted
52
53
54
55
56
57
58
59
60

fluoronitrobenzene afforded intermediates **38a-d**. Suzuki coupling between **38a-d** and pinacol boronic ester **37a-d** followed by hydrogenation of the nitro group yielded compounds **39a-d**, which then reacted with substituted amines to afford the target molecules.

Scheme 1. Synthesis of Compounds **14-27**^a



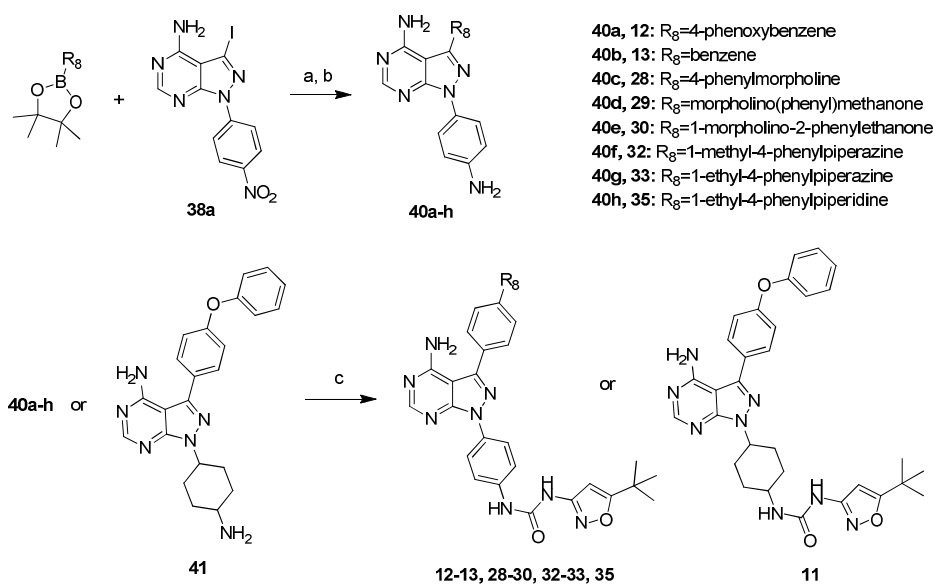
- 36a-39a, 14:** R₁=2-morpholinoethyl, R₂=R₃=R₅=H, R₄=NO₂, R₆=NH₂, R₇=5-(*tert*-butyl)isoxazole
36a, 37d, 38a-39a, 15: R₁=2-morpholinoethyl, R₂=R₃=R₅=H, R₄=NO₂, R₆=NH₂, R₇=5-(*tert*-butyl)isoxazole
36a-37a, 38b-39b, 16: R₁=2-morpholinoethyl, R₂=R₄=R₆=H, R₃=NO₂, R₅=NH₂, R₇=5-(*tert*-butyl)isoxazole
36a-39a, 17: R₁=2-morpholinoethyl, R₂=R₃=R₅=H, R₄=NO₂, R₆=NH₂, R₇=5-methylisoxazole
36a-39a, 18: R₁=2-morpholinoethyl, R₂=R₃=R₅=H, R₄=NO₂, R₆=NH₂, R₇=isoxazole
36a-39a, 19: R₁=2-morpholinoethyl, R₂=R₃=R₅=H, R₄=NO₂, R₆=NH₂, R₇=4-(*tert*-butyl)thiazole
36a-39a, 20: R₁=2-morpholinoethyl, R₂=R₃=R₅=H, R₄=NO₂, R₆=NH₂, R₇=4-(trifluoromethyl)thiazole
36a-39a, 21: R₁=2-morpholinoethyl, R₂=R₃=R₅=H, R₄=NO₂, R₆=NH₂, R₇=4-butylbenzene
36a-39a, 22: R₁=2-morpholinoethyl, R₂=R₃=R₅=H, R₄=NO₂, R₆=NH₂, R₇=4-(*tert*-butyl)-3-(trifluoromethyl)benzene
36a-39a, 23: R₁=2-morpholinoethyl, R₂=R₃=R₅=H, R₄=NO₂, R₆=NH₂, R₇=3,4,5-trimethoxybenzene
36a-37a, 38c-39c, 24: R₁=2-morpholinoethyl, R₂=R₅=H, R₃=Me, R₄=NO₂, R₆=NH₂, R₇=5-(*tert*-butyl)isoxazole
36a-37a, 38d-39d, 25: R₁=2-morpholinoethyl, R₃=R₅=H, R₂=Me, R₄=NO₂, R₆=NH₂, R₇=5-(*tert*-butyl)isoxazole
36b-37b, 38a-39a, 26: R₁=3-morpholinopropyl, R₂=R₃=R₅=H, R₄=NO₂, R₆=NH₂, R₇=5-(*tert*-butyl)isoxazole
36c-37c, 38a-39a, 27: R₁=2-piperidineethyl, R₂=R₃=R₅=H, R₄=NO₂, R₆=NH₂, R₇=5-(*tert*-butyl)isoxazole

1
2
3
4
5
6
7
8
9
10
11
12
13
14
15
16
17
18
19
20
21
22
23
24
25
26
27
28
29
30
31
32
33
34
35
36
37
38
39
40
41
42
43
44
45
46
47
48
49
50
51
52
53
54
55
56
57
58
59
60

^aReagents and conditions: (a) methanesulfonyl chloride, DIEPA, THF, 0 °C-rt, overnight, yield: 87.3%; (b) K₂CO₃, DMF, 70 °C, 8 h, yield: 74.3-75.6%; (c) for **38a**, **c-d**, K₂CO₃, DMF, 100 °C, overnight; for **38b**, K₂CO₃, DMF, 120 °C, overnight, yield: 80.1-82.5%; (d) **37a-d**, Pd(PPh₃)₄, K₂CO₃, 1,4-dioxane/H₂O, 90 °C, 12 h; (e) 10 % Pd/C, H₂, MeOH, rt, 4 h, two-step yield: 85.4-87.8%; (f) triphosgene, Et₃N, CH₂Cl₂, -10 to 25 °C, 16 h, yield: 48.9-55.3%.

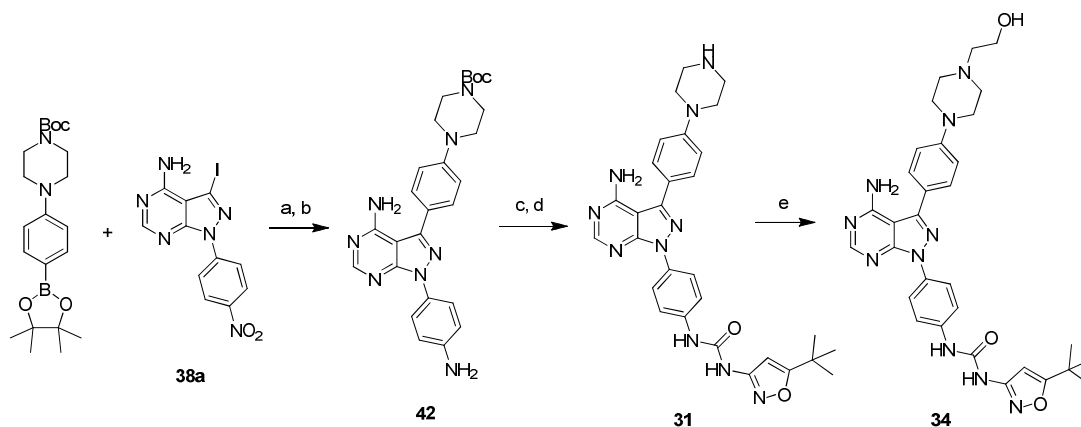
Similarly, Pd-catalyzed Suzuki coupling between **38a** and a series of substituted pinacol boronic esters following by hydrogenation reaction generated intermediates **40a-h**. Then compounds **40a-h** or **41** reacted with 5-(*tert*-butyl)isoxazol-3-amine to yield the desired products as shown in Scheme 2. Compound **31** was prepared following the same synthetic procedure except that the Boc group was deprotected under acidic condition as the last step (Scheme 3). Compound **34** was obtained from nucleophilic substitution of **31** with 2-iodoethanol.

Scheme 2. Synthesis of Compounds **11-13**, **28-30**, **32-33** and **35^a**



^aReagents and conditions: (a) Pd(PPh₃)₄, K₂CO₃, 1,4-dioxane/H₂O, 90 °C, 12 h; (b) 10 % Pd/C, H₂, MeOH, rt, 2 h, two-step yield: 84.6-88.2%; (c) 5-(*tert*-butyl)isoxazol-3-amine, triphosgene, Et₃N, CH₂Cl₂, -10 to 25 °C, 16 h, yield: 50.4-70.1%.

Scheme 3. Synthesis of Compounds **31** and **34**^a



^aReagents and conditions: (a) Pd(PPh₃)₄, K₂CO₃, 1,4-dioxane/H₂O, 90 °C, 12 h; (b) 10 % Pd/C, H₂, MeOH, rt, 2 h, two-step yield: 52.7%; (c) 5-(*tert*-butyl)isoxazol-3-amine, triphosgene, Et₃N, CH₂Cl₂, -10 to 25 °C, 16 h; (d) 4 N HCl in EtOAc, rt, 2 h, two-step yield: 52.7%; (e) 2-iodoethanol, K₂CO₃, DMF, rt, 3h, yield: 71.4%.

CONCLUSIONS

Starting from BTK kinase inhibitor compound **9**, which adopted a type I binding mode with FLT3 kinase and exhibited selective moderate activity against FLT3-ITD mutant in AML cancer cell lines, through a structure-guided drug design approach, we have discovered compound **14**, a novel type II FLT3 kinase inhibitor which exhibited high potency against FLT3-ITD mutant and other oncogenic mutations of FLT3 kinase especially drug resistant gatekeeper mutant F691L. Compound **14** selectively inhibited

1
2
3 the growth of FLT3-ITD positive AML cancer cell lines through strongly suppressing the
4
5 FLT3 mediated signaling pathways, arresting cell cycle and induction of apoptosis.
6
7
8 Compound **14** also displayed suitable PK properties and strong in vivo antitumor activity.
9
10
11 Meanwhile, it is worthy to note that compound **14** could also potently inhibit cKIT kinase
12
13 and CDK8/11 kinases. However, simultaneous inhibition of FLT3 kinase and cKIT
14
15 kinase might induce the myelosuppression toxicity and inhibition of CDK8/11 kinase has
16
17 the risk of pleiotropic toxicity. Therefore, careful safety attention should be paid when
18
19 the inhibitor is moved to the clinical trial. In summary, all these reported results
20
21 suggested that compound **14** might be a potential drug candidate for FLT3-ITD driven
22
23
24
25
26
27
28
29
30
31
32
33
34
35
36
37
38
39
40
41
42
43
44
45
46
47
48
49
50
51
52
53
54
55
56
57
58
59
60
AML.

EXPERIMENTAL SECTION

Chemistry. All solvents and reagents were used as obtained. ^1H and ^{13}C NMR spectra were recorded with a Bruker 400 MHz NMR spectrometer and referenced to deuterium dimethyl sulfoxide ($\text{DMSO-}d_6$) or deuterium chloroform (CDCl_3). Chemical shifts are expressed in ppm. In the NMR tabulation, s indicates singlet; d, doublet; t, triplet; q, quartet; m, multiplet; and br, broad peak. LC/MS experiments were performed on an Agilent 6224 TOF using an ESI source coupled to an Agilent 1260 Infinity HPLC system operating in reverse mode with an Agilent Eclipse Plus C18 1.8 μm , 3.0 mm \times 50 mm column. Purification of the final compounds were performed with an Isco CombiFlash Rf+ system (silica flash column 4 g) using a gradient of 0-10 % MeOH in DCM over 20 min at a flow rate of 18 mL/min. The purities of all final compounds were above 95 %.

Compounds **11-30**, **32-33**, **35** were prepared following the synthetic procedure of compound **14**.

1
2
3
4
5
6
7
8
9
10
11
12
13
14
15
16
17
18
19
20
21
22
23
24
25
26
27
28
29
30
31
32
33
34
35
36
37
38
39
40
41
42
43
44
45
46
47
48
49
50
51
52
53
54
55
56
57
58
59
60

1-(4-(4-Amino-3-(4-phenoxyphenyl)-1H-pyrazolo[3,4-d]pyrimidin-1-yl)cyclohexyl)-3-(5-(tert-butyl)isoxazol-3-yl)urea (11). Yield =70.1%. ¹H NMR (400 MHz, DMSO-*d*₆) δ 9.24 (s, 1H), 8.26 (s, 1H), 7.68 (s, 2H), 7.45 (s, 2H), 7.17 (s, 5H), 6.95 (s, 1H), 6.39 (s, 1H), 4.77 (s, 1H), 3.93 (s, 2H), 2.16 (s, 2H), 1.87 (s, 5H), 1.27 (s, 9H); LC/MS (ESI, m/z) 567.28 [M + H]⁺.

1-(4-(4-Amino-3-(4-phenoxyphenyl)-1H-pyrazolo[3,4-d]pyrimidin-1-yl)phenyl)-3-(5-(tert-butyl)isoxazol-3-yl)urea (12). Yield =52.5%. ¹H NMR (400 MHz, DMSO-*d*₆) δ 9.70 (s, 1H), 9.37 (s, 1H), 8.37 (s, 1H), 8.13 (d, *J* = 8.4 Hz, 2H), 7.77 (d, *J* = 8.5 Hz, 3H), 7.65 (d, *J* = 9.0 Hz, 1H), 7.59 – 7.41 (m, 2H), 7.18 (dd, *J* = 15.5, 7.9 Hz, 5H), 6.55 (s, 1H), 1.31 (s, 9H); LC/MS (ESI, m/z) 563.23 [M + H]⁺.

1-(4-(4-Amino-3-phenyl-1H-pyrazolo[3,4-d]pyrimidin-1-yl)phenyl)-3-(5-(tert-butyl)isoxazol-3-yl)urea (13). Yield =53.3%. ¹H NMR (400 MHz, DMSO-*d*₆) δ 9.58 (s, 1H), 9.04 (s, 1H), 8.39 (s, 1H), 8.14 (s, 2H), 7.77 (s, 2H), 7.62 (d, *J* = 14.9 Hz, 5H), 6.55 (s, 1H), 1.31 (s, 9H); LC/MS (ESI, m/z) 469.21 [M + H]⁺.

1-(4-(4-Amino-3-(4-(2-morpholinoethoxy)phenyl)-1H-pyrazolo[3,4-d]pyrimidin-1-yl)phenyl)-3-(5-(tert-butyl)isoxazol-3-yl)urea (14) A solution of **39a** (50 mg, 0.12 mmol) and Et₃N (14 mg, 0.14 mmol) in DCM (2 mL) was added dropwise to a cooled solution (−10 °C) of triphosgene (11 mg, 0.04 mmol) in DCM (2 mL). The mixture was stirred for 1 h at room temperature followed by addition of a solution of 5-(*tert*-butyl)isoxazol-3-amine (16 mg, 0.12 mmol) and Et₃N (14 mg, 0.14 mmol) in DCM (2 mL). The mixture was then stirred for 16 h at room temperature. The resulting mixture was concentrated and purified with the CombiFlash system (0-10% MeOH in DCM) to afford title compound **14** (35 mg, 50.7%) as a white solid. ¹H NMR (400 MHz, DMSO-*d*₆) δ 9.55 (s,

1
2
3 1H), 8.99 (s, 1H), 8.36 (s, 1H), 8.13 (s, 2H), 7.65 (s, 4H), 7.14 (s, 2H), 6.54 (s, 1H), 4.17
4
5 (s, 2H), 3.59 (s, 4H), 2.73 (s, 2H), 2.50 (s, 4H), 1.30 (s, 9H); ¹³C NMR (100 MHz,
6
7 DMSO-*d*₆) δ 180.69, 159.60, 158.83, 156.88, 154.43, 151.82, 145.46, 137.53, 134.00,
8
9 130.25, 125.12, 122.09, 119.34, 115.67, 99.03, 92.95, 66.66, 65.98, 57.45, 54.10, 32.95,
10
11 28.83; LC/MS (ESI, m/z) 598.28 [M + H]⁺.

12
13
14
15 *1-(4-(4-Amino-3-(3-(2-morpholinoethoxy)phenyl)-1H-pyrazolo[3,4-d]pyrimidin-1-*
16
17 *yl)phenyl)-3-(5-(tert-butyl)isoxazol-3-yl)urea (15)*. Yield =48.9%. ¹H NMR (400 MHz,
18
19 DMSO-*d*₆) δ 9.71 (s, 1H), 9.35 (s, 1H), 8.38 (s, 1H), 8.12 (s, 2H), 7.65 (s, 2H), 7.50 (s,
20
21 1H), 7.32 (s, 2H), 7.13 (s, 1H), 6.55 (s, 1H), 4.24 (s, 2H), 3.63 (s, 4H), 2.85 (s, 2H), 2.61
22
23 (s, 4H), 1.31 (s, 9H); LC/MS (ESI, m/z) 598.28 [M + H]⁺.

24
25
26
27 *1-(3-(4-Amino-3-(4-(2-morpholinoethoxy)phenyl)-1H-pyrazolo[3,4-d]pyrimidin-1-*
28
29 *yl)phenyl)-3-(5-(tert-butyl)isoxazol-3-yl)urea (16)*. Yield =54.6%. ¹H NMR (400 MHz,
30
31 DMSO-*d*₆) δ 9.64 (s, 1H), 9.44 (s, 1H), 8.38 (s, 2H), 7.96 (s, 1H), 7.69 (s, 2H), 7.44 (s,
32
33 2H), 7.19 (s, 2H), 6.55 (s, 1H), 4.25 (s, 2H), 3.66 (s, 4H), 2.83 (s, 2H), 2.63 (s, 4H), 1.30
34
35 (s, 9H); LC/MS (ESI, m/z) 598.28 [M + H]⁺.

36
37
38
39 *1-(4-(4-Amino-3-(4-(2-morpholinoethoxy)phenyl)-1H-pyrazolo[3,4-d]pyrimidin-1-*
40
41 *yl)phenyl)-3-(5-methylisoxazol-3-yl)urea (17)*. Yield =51.3%. ¹H NMR (400 MHz,
42
43 DMSO-*d*₆) δ 9.72 (s, 1H), 9.53 (s, 1H), 8.37 (s, 1H), 8.24 (s, 2H), 8.12 (s, 2H), 7.69 (s,
44
45 2H), 7.18 (s, 2H), 6.59 (s, 1H), 4.26 (s, 2H), 3.66 (s, 4H), 2.90 (s, 2H), 2.66 (s, 4H), 2.38
46
47 (s, 3H); LC/MS (ESI, m/z) 556.24 [M + H]⁺.

48
49
50
51 *1-(4-(4-Amino-3-(4-(2-morpholinoethoxy)phenyl)-1H-pyrazolo[3,4-d]pyrimidin-1-*
52
53 *yl)phenyl)-3-(isoxazol-3-yl)urea (18)*. Yield =54.2%. ¹H NMR (400 MHz, DMSO-*d*₆) δ
54
55 9.99 (s, 1H), 9.80 (s, 1H), 8.75 (s, 1H), 8.37 (s, 1H), 8.12 (s, 2H), 7.66 (s, 2H), 7.44 (s,
56
57
58
59
60

2H), 7.20 (s, 2H), 6.89 (s, 1H), 4.48 (s, 2H), 3.85 (s, 4H), 2.81 (s, 2H), 2.62 (s, 4H);
LC/MS (ESI, m/z) 542.22 [M + H]⁺.

1-(4-(4-Amino-3-(4-(2-morpholinoethoxy)phenyl)-1H-pyrazolo[3,4-d]pyrimidin-1-yl)phenyl)-3-(4-(tert-butyl)thiazol-2-yl)urea (19). Yield =48.1%. ¹H NMR (400 MHz, DMSO-*d*₆) δ 9.71 (s, 1H), 8.37 (s, 1H), 8.14 (s, 2H), 7.67 (s, 4H), 7.17 (s, 3H), 6.65 (s, 1H), 4.22 (s, 2H), 3.62 (s, 4H), 2.80 (s, 2H), 2.50 (s, 4H), 1.26 (s, 9H); LC/MS (ESI, m/z) 614.26 [M + H]⁺.

1-(4-(4-Amino-3-(4-(2-morpholinoethoxy)phenyl)-1H-pyrazolo[3,4-d]pyrimidin-1-yl)phenyl)-3-(4-(trifluoromethyl)thiazol-2-yl)urea (20). Yield =48.9%. ¹H NMR (400 MHz, DMSO-*d*₆) δ 10.17 (s, 1H), 8.38 (s, 1H), 8.17 (s, 2H), 7.87 (s, 1H), 7.70 (s, 4H), 7.20 (s, 3H), 4.36 (s, 2H), 3.75 (s, 4H), 3.13 (s, 2H), 2.90 (s, 4H); LC/MS (ESI, m/z) 626.19 [M + H]⁺.

1-(4-(4-Amino-3-(4-(2-morpholinoethoxy)phenyl)-1H-pyrazolo[3,4-d]pyrimidin-1-yl)phenyl)-3-(4-butylphenyl)urea (21). Yield =50.5%. ¹H NMR (400 MHz, DMSO) δ 9.89 (s, 1H), 9.66 (s, 1H), 8.35 (s, 1H), 8.04 (s, 2H), 7.68-7.49 (m, 6H), 7.18 (s, 2H), 7.08 (s, 2H), 4.36 (s, 2H), 3.75 (s, 4H), 3.40 (s, 5H), 3.16 (s, 1H), 2.50 (s, 2H), 1.52 (s, 2H), 1.25 (s, 2H), 0.89 (s, 3H); LC/MS (ESI, m/z) 607.31 [M + H]⁺.

1-(4-(4-Amino-3-(4-(2-morpholinoethoxy)phenyl)-1H-pyrazolo[3,4-d]pyrimidin-1-yl)phenyl)-3-(4-methyl-3-(trifluoromethyl)phenyl)urea (22). Yield =47.5%. ¹H NMR (400 MHz, DMSO-*d*₆) δ 10.03 (s, 1H), 9.85 (s, 1H), 8.35 (s, 1H), 8.11 (s, 2H), 7.95 (s, 1H), 7.66 (s, 4H), 7.54 (s, 1H), 7.20 (s, 3H), 4.23 (s, 2H), 3.64 (s, 4H), 2.86 (s, 2H), 2.62 (s, 4H), 2.36 (s, 3H); LC/MS (ESI, m/z) 633.25 [M + H]⁺.

1
2
3
4
5
6
7
8
9
10
11
12
13
14
15
16
17
18
19
20
21
22
23
24
25
26
27
28
29
30
31
32
33
34
35
36
37
38
39
40
41
42
43
44
45
46
47
48
49
50
51
52
53
54
55
56
57
58
59
60

1-(4-(4-Amino-3-(4-(2-morpholinoethoxy)phenyl)-1H-pyrazolo[3,4-d]pyrimidin-1-yl)phenyl)-3-(3,4,5-trimethoxyphenyl)urea (23). Yield =55.3%. ¹H NMR (400 MHz, DMSO-*d*₆) δ 9.33 (s, 1H), 9.17 (s, 1H), 8.36 (s, 1H), 8.22 (s, 2H), 8.08 (s, 2H), 7.69 (s, 2H), 7.18 (s, 2H), 6.84 (s, 2H), 4.26 (s, 2H), 3.77 (s, 6H), 3.64 (d, *J* = 13.6 Hz, 4H), 2.90 (s, 2H), 2.66 (s, 4H); LC/MS (ESI, *m/z*) 641.28 [M + H]⁺.

1-(4-(4-Amino-3-(4-(2-morpholinoethoxy)phenyl)-1H-pyrazolo[3,4-d]pyrimidin-1-yl)-2-methylphenyl)-3-(5-(tert-butyl)isoxazol-3-yl)urea (24). Yield =51.8%. ¹H NMR (400 MHz, DMSO-*d*₆) δ 10.09 (s, 1H), 8.59 (s, 1H), 8.37 (s, 1H), 8.02 (s, 3H), 7.69 (s, 2H), 7.17 (s, 2H), 6.51 (s, 1H), 4.24 (s, 2H), 3.65 (s, 4H), 2.86 (s, 2H), 2.62 (s, 4H), 2.36 (s, 3H), 1.31 (s, 9H); LC/MS (ESI, *m/z*) 612.30 [M + H]⁺.

1-(4-(4-Amino-3-(4-(2-morpholinoethoxy)phenyl)-1H-pyrazolo[3,4-d]pyrimidin-1-yl)-3-methylphenyl)-3-(5-(tert-butyl)isoxazol-3-yl)urea (25). Yield =51.4%. ¹H NMR (400 MHz, DMSO-*d*₆) δ 9.77 (s, 1H), 9.42 (s, 1H), 8.24 (s, 1H), 7.68 (s, 2H), 7.55 (s, 1H), 7.46 (s, 1H), 7.35 (s, 1H), 7.17 (s, 2H), 6.56 (s, 1H), 4.33 (s, 2H), 3.73 (s, 4H), 3.10 (s, 2H), 2.85 (s, 4H), 2.09 (s, 3H), 1.29 (s, 9H); LC/MS (ESI, *m/z*) 612.30 [M + H]⁺.

1-(4-(4-Amino-3-(4-(3-morpholinopropoxy)phenyl)-1H-pyrazolo[3,4-d]pyrimidin-1-yl)phenyl)-3-(5-(tert-butyl)isoxazol-3-yl)urea (26). Yield =52.7%. ¹H NMR (400 MHz, DMSO-*d*₆) δ 9.70 (s, 1H), 9.34 (s, 1H), 8.37 (s, 1H), 8.12 (s, 2H), 7.71 (s, 2H), 7.65 (s, 2H), 7.17 (s, 2H), 6.55 (s, 1H), 4.17 (s, 2H), 3.86 (s, 4H), 3.21 (s, 4H), 2.21 (s, 2H), 1.29 (s, 9H); LC/MS (ESI, *m/z*) 612.30 [M + H]⁺.

1-(4-(4-Amino-3-(4-(2-(piperidin-1-yl)ethoxy)phenyl)-1H-pyrazolo[3,4-d]pyrimidin-1-yl)phenyl)-3-(5-(tert-butyl)isoxazol-3-yl)urea (27). Yield =53.4%. ¹H NMR (400 MHz, DMSO-*d*₆) δ 10.31 (s, 1H), 10.06 (s, 1H), 8.35 (s, 1H), 8.09 (s, 2H), 7.70-7.49 (m, 4H),

7.21 (s, 2H), 6.55 (s, 1H), 4.56 (s, 2H), 3.49-3.40 (m, 6H), 1.83 (s, 4H), 1.55 (s, 2H), 1.29 (s, 9H); LC/MS (ESI, m/z) 596.30 [M + H]⁺.

1-(4-(4-Amino-3-(4-morpholinophenyl)-1H-pyrazolo[3,4-d]pyrimidin-1-yl)phenyl)-3-(5-(tert-butyl)isoxazol-3-yl)urea (28). Yield =50.6%. ¹H NMR (400 MHz, DMSO-*d*₆) δ 9.75 (s, 1H), 9.50 (s, 1H), 8.36 (s, 1H), 8.13 (s, 2H), 7.64 (s, 3H), 7.16 (s, 3H), 6.56 (s, 1H), 3.79 (s, 3H), 3.33 (s, 2H), 3.25 (s, 3H), 1.32 (s, 9H); LC/MS (ESI, m/z) 554.26 [M + H]⁺.

1-(4-(4-Amino-3-(4-(morpholine-4-carbonyl)phenyl)-1H-pyrazolo[3,4-d]pyrimidin-1-yl)phenyl)-3-(5-(tert-butyl)isoxazol-3-yl)urea (29). Yield =52.4%. ¹H NMR (400 MHz, DMSO-*d*₆) δ 9.83 (s, 1H), 9.41 (s, 1H), 8.39 (s, 1H), 8.11 (s, 2H), 7.82 (s, 2H), 7.65 (s, 2H), 7.60 (s, 2H), 6.56 (s, 1H), 6.36 (s, 1H), 3.65-3.48 (m, 8H), 1.29 (s, 9H); LC/MS (ESI, m/z) 582.25 [M + H]⁺.

1-(4-(4-Amino-3-(4-(2-morpholino-2-oxoethyl)phenyl)-1H-pyrazolo[3,4-d]pyrimidin-1-yl)phenyl)-3-(5-(tert-butyl)isoxazol-3-yl)urea (30). Yield =51.5%. ¹H NMR (400 MHz, DMSO-*d*₆) δ 9.90 (s, 2H), 8.38 (s, 1H), 8.11 (s, 2H), 7.72 (s, 2H), 7.66 (s, 2H), 7.45 (s, 2H), 6.56 (s, 1H), 3.84 (s, 2H), 3.55-3.50 (m, 8H), 1.31 (s, 9H); LC/MS (ESI, m/z) 596.27 [M + H]⁺.

1-(4-(4-Amino-3-(4-(piperazin-1-yl)phenyl)-1H-pyrazolo[3,4-d]pyrimidin-1-yl)phenyl)-3-(5-(tert-butyl)isoxazol-3-yl)urea (31). A solution of **42** (100 mg, 0.20 mmol) and Et₃N (24 mg, 0.24 mmol) in DCM (2 mL) was added dropwise to a cooled solution (-10 °C) of triphosgene (18.2 mg, 0.06 mmol) in DCM (4 mL). The mixture was stirred for 1 h at room temperature followed by addition of a solution of 5-(*tert*-butyl)isoxazol-3-amine (24 mg, 0.24 mmol) and Et₃N (24mg, 0.24 mmol) in DCM (4 mL). The mixture

1
2
3 was then stirred for 16 h at room temperature. The resulting mixture was concentrated
4 and purified with the CombiFlash system (0-10% MeOH in DCM) to afford the desired
5 Boc-protected intermediate **42** (61 mg) as an off-white solid. Then, to the solid in EtOAc
6 (2 mL) was added 4 N HCl in EtOAc (4 mL). The reaction mixture was stirred at room
7 temperature for 1 h. After complete conversion of the starting material, excess EtOAc
8 was removed under vacuum. The residue was diluted in EtOAc and water. The water
9 layer was basified with 2 N NaHCO₃ solution and extracted with EtOAc (3 × 30 mL).
10 The organic layers were then washed with water followed by brine. The organic layers
11 were dried over sodium sulfate, filtered, concentrated and purified with the CombiFlash
12 system (0-10% MeOH in DCM) to afford compound **31** (27 mg, 51.9%) as a white solid.
13 ¹H NMR (400 MHz, DMSO-*d*₆) δ 9.90 (s, 2H), 8.36 (s, 1H), 8.11 (s, 2H), 7.65 (s, 3H),
14 7.21 (s, 3H), 6.56 (s, 1H), 3.55 (s, 4H), 3.24 (s, 3H), 3.12 (s, 2H), 1.31 (s, 9H); LC/MS
15 (ESI, m/z) 533.27 [M + H]⁺.
16
17
18
19
20
21
22
23
24
25
26
27
28
29
30
31
32
33

34 *1-(4-(4-Amino-3-(4-(4-methylpiperazin-1-yl)phenyl)-1H-pyrazolo[3,4-d]pyrimidin-1-*
35 *yl)phenyl)-3-(5-(tert-butyl)isoxazol-3-yl)urea (32)*. Yield =50.7%. ¹H NMR (400 MHz,
36 DMSO-*d*₆) δ 9.94 (s, 1H), 8.55 (s, 1H), 8.10 (s, 1H), 7.65 (s, 3H), 7.42 (s, 3H), 7.21 (s,
37 2H), 6.55 (s, 1H), 3.60 (s, 3H), 3.27 (s, 3H), 2.76 (s, 2H), 2.51 (s, 3H) 1.30 (s, 9H);
38 LC/MS (ESI, m/z) 567.29 [M + H]⁺.
39
40
41
42
43
44
45

46 *1-(4-(4-Amino-3-(4-(4-ethylpiperazin-1-yl)phenyl)-1H-pyrazolo[3,4-d]pyrimidin-1-*
47 *yl)phenyl)-3-(5-(tert-butyl)isoxazol-3-yl)urea (33)*. Yield =54.1%. ¹H NMR (400 MHz,
48 DMSO-*d*₆) δ 9.86 (s, 1H), 9.78 (s, 1H), 8.56 (s, 2H), 8.36 (s, 1H), 8.12 (s, 2H), 7.65 (s,
49 2H), 7.22 (s, 2H), 6.55 (s, 1H), 3.62 (s, 4H), 3.29 (s, 4H), 3.13 (s, 2H), 1.31 (s, 12H);
50 LC/MS (ESI, m/z) 581.31 [M + H]⁺.
51
52
53
54
55
56
57
58
59
60

1
2
3
4
5
6
7
8
9
10
11
12
13
14
15
16
17
18
19
20
21
22
23
24
25
26
27
28
29
30
31
32
33
34
35
36
37
38
39
40
41
42
43
44
45
46
47
48
49
50
51
52
53
54
55
56
57
58
59
60

1-(4-(4-Amino-3-(4-(4-(2-hydroxyethyl)piperazin-1-yl)phenyl)-1H-pyrazolo[3,4-d]pyrimidin-1-yl)phenyl)-3-(5-(tert-butyl)isoxazol-3-yl)urea (34). To a solution of **31** (20 mg, 0.03 mmol) in DMF (2 mL) was added K₂CO₃ (10mg, 0.06mmol) and 2-iodoethanol (6.5mg, 0.03mmol). The resulting mixture was stirred at room temperature for 3 h, and then diluted with EtOAc and washed with water followed by brine. The organic layers were dried over sodium sulfate, filtered, concentrated and purified with the CombiFlash system (0-10% MeOH in DCM) to afford title compound **34** (15 mg, 71.4%) as a white solid. ¹H NMR (400 MHz, DMSO-*d*₆) δ 9.76 (s, 1H), 9.54 (s, 1H), 8.36 (s, 1H), 8.12 (s, 2H), 7.65 (s, 4H), 7.20 (s, 3H), 6.55 (s, 1H), 3.77 (s, 2H), 3.34 (s, 6H), 3.10 (s, 4H), 1.32 (s, 9H); LC/MS (ESI, m/z) 597.30 [M + H]⁺.

1-(4-(4-Amino-3-(4-(1-ethylpiperidin-4-yl)phenyl)-1H-pyrazolo[3,4-d]pyrimidin-1-yl)phenyl)-3-(5-(tert-butyl)isoxazol-3-yl)urea (35). Yield =50.4%. ¹H NMR (400 MHz, DMSO-*d*₆) δ 9.62 (s, 1H), 9.19 (s, 1H), 8.38 (s, 1H), 8.14 (s, 2H), 7.74 (s, 2H), 7.66 (s, 2H), 7.49 (s, 2H), 6.54 (s, 1H), 2.77 (s, 3H), 1.94 (s, 4H), 1.31 (s, 13H) 1.16 (s, 3H); LC/MS (ESI, m/z) 580.31 [M + H]⁺.

2-Morpholinoethyl methanesulfonate (36a) To a solution of 2-morpholinoethanol (5 g, 38.1mmol) in THF (30 mL) were added DIEPA (5.9 g, 45.8 mmol) and methanesulfonyl chloride (4.8 g, 41.9 mol) at 0 °C. The resulting mixture was stirred overnight at room temperature. Then it was diluted with EtOAc and washed with water followed by brine. The organic layers were dried over sodium sulfate, filtered, and concentrated to provide **36a** as a light yellow oil (6.9 g, 87.3%), which was used directly without further purification.

Compounds **36b–c** were prepared following the synthetic procedure of **36a**.

1
2
3
4
5
6
7
8
9
10
11
12
13
14
15
16
17
18
19
20
21
22
23
24
25
26
27
28
29
30
31
32
33
34
35
36
37
38
39
40
41
42
43
44
45
46
47
48
49
50
51
52
53
54
55
56
57
58
59
60

4-(2-(4-(4,4,5,5-Tetramethyl-1,3,2-dioxaborolan-2-yl)phenoxy)ethyl)morpholine

(**37a**) A mixture of **36a** (6.9 g, 33.0 mmol), 4-(4,4,5,5-tetramethyl-1,3,2-dioxaborolan-2-yl)phenol (8.7 g, 39.6 mmol) and K₂CO₃ (9.1 g, 66.0 mmol) in DMF (80 mL) was stirred at 70 °C for 8 h. The resulting mixture was diluted with 500 mL EtOAc and then washed with water (3 × 80 mL) followed by brine. The organic layers were dried over sodium sulfate, filtered, concentrated and purified by silica gel column chromatography (eluting with 0–2% MeOH in DCM) to afford **37a** (8.1 g, 74.3%) as a light purple solid. ¹H NMR (400 MHz, DMSO-*d*₆) δ 7.60 (s, 2H), 6.93 (s, 2H), 4.11 (s, 2H), 3.57 (s, 4H), 2.89 (s, 1H), 2.74-2.69 (m, 3H), 1.28 (s, 12H); LC/MS (ESI, *m/z*) 334.21 [M + H]⁺.

Compounds **37b–d** were prepared following the synthetic procedure of **37a**.

4-(3-(4-(4,4,5,5-Tetramethyl-1,3,2-dioxaborolan-2-yl)phenoxy)propyl)morpholine

(**37b**) Yield =73.5%. ¹H NMR (400 MHz, CDCl₃) δ 7.76 (s, 2H), 6.91 (s, 2H), 4.07 (s, 2H), 3.74 (s, 4H), 2.54-2.49 (m, 6H), 1.99 (s, 2H), 1.35 (s, 12H); LC/MS (ESI, *m/z*) 338.23 [M + H]⁺.

1-(2-(4-(4,4,5,5-Tetramethyl-1,3,2-dioxaborolan-2-yl)phenoxy)ethyl)piperidine (37c)

Yield =75.6%. ¹H NMR (400 MHz, CDCl₃) δ 7.71 (s, 2H), 6.87 (s, 2H), 4.28 (s, 2H), 3.01 (s, 2H), 2.77 (s, 4H), 1.76 (s, 4H), 1.50 (s, 2H), 1.30 (s, 12H); LC/MS (ESI, *m/z*) 332.23 [M + H]⁺.

4-(2-(3-(4,4,5,5-Tetramethyl-1,3,2-dioxaborolan-2-yl)phenoxy)ethyl)morpholine

(**37d**) Yield =74.7%. ¹H NMR (400 MHz, DMSO-*d*₆) δ 7.27-7.05 (m, 4H), 4.07 (s, 2H), 3.57 (s, 6H), 2.95 – 2.59 (m, 4H), 1.27 (s, 12H); LC/MS (ESI, *m/z*) 334.21 [M + H]⁺.

3-Iodo-1-(4-nitrophenyl)-1H-pyrazolo[3,4-d]pyrimidin-4-amine (38a) To a solution of 3-iodo-1H-pyrazolo[3,4-d]pyrimidin-4-amine (10.0 g, 38.3 mmol) in DMF (100 mL)

1
2
3 were added K₂CO₃ (15.8 g, 114.9 mmol) and 1-fluoro-4-nitrobenzene (5.9 g, 42.1 mmol).
4
5 After the resulting mixture was stirred overnight at 100 °C under N₂ atmosphere, the
6
7 reaction mixture was cooled to rt before pouring into water (500 mL). The precipitate
8
9 was collected, washed with water, and dried to provide **38a** (11.8 g, 80.8%) as a light
10
11 yellow solid. ¹H NMR (400 MHz, DMSO-*d*₆) δ 8.50 (s, 2H), 8.39 (s, 2H), 8.20 (s, 1H);
12
13 LC/MS (ESI, m/z) 382.97 [M + H]⁺.
14
15

16
17 Compounds **38b–d** were prepared following the synthetic procedure of **38a**.
18

19
20 *3-Iodo-1-(3-nitrophenyl)-1H-pyrazolo[3,4-d]pyrimidin-4-amine (38b)* Yield =81.6%.
21
22 ¹H NMR (400 MHz, DMSO-*d*₆) δ 9.06 (s, 1H), 8.60 (s, 1H), 8.39 (s, 1H), 8.17 (s, 1H),
23
24 7.83 (s, 1H); LC/MS (ESI, m/z) 382.97 [M + H]⁺.
25
26

27 *3-Iodo-1-(3-methyl-4-nitrophenyl)-1H-pyrazolo[3,4-d]pyrimidin-4-amine (38c)*
28
29 Yield =80.1%. ¹H NMR (400 MHz, DMSO-*d*₆) δ 8.37 (s, 1H), 8.28 (d, *J* = 12.1 Hz, 2H),
30
31 8.19 (s, 1H), 2.62 (s, 3H); LC/MS (ESI, m/z) 396.99 [M + H]⁺.
32
33

34 *3-Iodo-1-(2-methyl-4-nitrophenyl)-1H-pyrazolo[3,4-d]pyrimidin-4-amine (38d)*
35
36 Yield =82.5%. ¹H NMR (400 MHz, DMSO-*d*₆) δ 8.36 (s, 1H), 8.24 (s, 2H), 7.73 (s, 1H),
37
38 2.28 (s, 3H); LC/MS (ESI, m/z) 396.99 [M + H]⁺.
39
40

41 *1-(4-Aminophenyl)-3-(4-(2-morpholinoethoxy)phenyl)-1H-pyrazolo[3,4-d]pyrimidin-*
42
43 *4-amine (39a)* To a mixture of **37a** (7.0 g, 20.0 mmol) and 1,4-dioxane/H₂O (50 mL, v/v,
44
45 5:1) were added **38a** (7.3 g, 19.1 mmol), K₂CO₃ (5.3 g, 38.2 mmol) and Pd(PPh₃)₄ (1.1 g,
46
47 0.9mmol). The reaction mixture was placed into an oil bath preheated to 90 °C with
48
49 stirring at this temperature for 12 h under argon. Then the reaction mixture was cooled to
50
51 rt before pouring into water (200 mL). The precipitate was collected, washed with water,
52
53 MeOH, and dried to provide the nitrobenzene intermediate as a yellow solid (7.1 g). Then
54
55
56
57
58
59
60

1
2
3 to the solid (7.0 g, 15.1 mmol) in MeOH (50 mL) was added Pd/C (1.0 g, 10 %) under H₂
4
5 atmosphere. The resulting mixture was stirred at rt for 4 h and then diluted with 100 mL
6
7 of DCM. The solid was filtered and the filtrate was evaporated. The residue was purified
8
9 by silica gel column chromatography (eluting with 0-4% MeOH in DCM) to provide **39a**
10
11 (5.8 g, 87.8%) as an off-white solid. ¹H NMR (400 MHz, DMSO-*d*₆) δ 8.29 (s, 1H), 7.66
12
13 (s, 4H), 7.16 (s, 2H), 6.70 (s, 2H), 5.37 (s, 2H), 4.38 (s, 2H), 3.78 (s, 4H), 3.40 (s, 2H),
14
15 3.16 (s, 2H), 2.96 (s, 2H).; LC/MS (ESI, m/z) 432.21 [M + H]⁺.
16
17
18
19

20 Compounds **39b-d**, **40a-h** and **42** were prepared following the synthetic procedure
21
22 of **39a**.
23

24
25 *1-(3-Aminophenyl)-3-(4-(2-morpholinoethoxy)phenyl)-1H-pyrazolo[3,4-d]pyrimidin-*
26
27 *4-amine (39b)* Yield =86.3%. ¹H NMR (400 MHz, DMSO-*d*₆) δ 8.34 (s, 1H), 7.68 (s,
28
29 2H), 7.42 (s, 4H), 7.17 (s, 2H), 5.39 (s, 2H), 4.39 (s, 2H), 3.78 (s, 4H), 3.45 (s, 2H), 2.96
30
31 (s, 4H); LC/MS (ESI, m/z) 432.21 [M + H]⁺.
32
33

34
35 *1-(4-Amino-3-methylphenyl)-3-(4-(2-morpholinoethoxy)phenyl)-1H-pyrazolo[3,4-*
36
37 *d]pyrimidin-4-amine (39c)* Yield =85.4%. ¹H NMR (400 MHz, DMSO-*d*₆) δ 8.29 (s, 1H),
38
39 7.66-7.59 (m, 5H), 7.16 (s, 2H), 6.75 (s, 1H), 5.11 (s, 2H), 4.34 (s, 4H), 3.73 (s, 15H),
40
41 3.45 (s, 2H), 2.85 (s, 4H), 2.14 (s, 3H); LC/MS (ESI, m/z) 446.23 [M + H]⁺.
42
43

44
45 *1-(4-Amino-2-methylphenyl)-3-(4-(2-morpholinoethoxy)phenyl)-1H-pyrazolo[3,4-*
46
47 *d]pyrimidin-4-amine (39d)* Yield =86.7%. ¹H NMR (400 MHz, DMSO-*d*₆) δ 8.19 (s,
48
49 1H), 7.64 (s, 2H), 7.15 (s, 2H), 6.99 (s, 1H), 6.55 (s, 2H), 5.36 (s, 2H), 4.35 (s, 2H), 3.75
50
51 (s, 2H), 3.37 (s, 2H), 3.15-2.89 (m, 4H), 1.89 (s, 3H); LC/MS (ESI, m/z) 446.23 [M +
52
53 H]⁺.
54
55
56
57
58
59
60

1
2
3
4
5
6
7
8
9
10
11
12
13
14
15
16
17
18
19
20
21
22
23
24
25
26
27
28
29
30
31
32
33
34
35
36
37
38
39
40
41
42
43
44
45
46
47
48
49
50
51
52
53
54
55
56
57
58
59
60

1-(4-Aminophenyl)-3-(4-phenoxyphenyl)-1H-pyrazolo[3,4-d]pyrimidin-4-amine

(**40a**) Yield =84.6%. ¹H NMR (400 MHz, DMSO-*d*₆) δ 8.30 (s, 1H), 7.72 (s, 4H), 7.44 (s, 4H), 7.16 (s, 5H), 5.32 (s, 2H); LC/MS (ESI, m/z) 395.16 [M + H]⁺.

1-(4-Aminophenyl)-3-phenyl-1H-pyrazolo[3,4-d]pyrimidin-4-amine (**40b**) Yield

=85.8%. ¹H NMR (400 MHz, DMSO-*d*₆) δ 8.31 (s, 1H), 7.75-7.70 (m, 5H), 7.58-7.54 (m, 4H), 5.39 (s, 2H); LC/MS (ESI, m/z) 303.13 [M + H]⁺.

1-(4-Aminophenyl)-3-(4-morpholinophenyl)-1H-pyrazolo[3,4-d]pyrimidin-4-amine

(**40c**) Yield =87.2%. ¹H NMR (400 MHz, DMSO-*d*₆) δ 8.28 (s, 1H), 7.68 (s, 2H), 7.59 (s, 2H), 7.12 (s, 2H), 6.70 (s, 2H), 5.39 (s, 2H), 3.76 (s, 4H), 3.21 (s, 4H); LC/MS (ESI, m/z) 388.18 [M + H]⁺.

(4-(4-Amino-1-(4-aminophenyl)-1H-pyrazolo[3,4-d]pyrimidin-3-

yl)phenyl)(morpholino)methanone (**40d**) Yield =86.9%. ¹H NMR (400 MHz, DMSO-*d*₆) δ 8.31 (s, 1H), 7.79 (s, 2H), 7.69 (s, 2H), 7.59 (s, 2H), 6.72 (s, 2H), 5.42 (s, 2H), 3.64 (s, 4H), 3.39 (s, 4H); LC/MS (ESI, m/z) 416.18 [M + H]⁺.

2-(4-(4-Amino-1-(4-aminophenyl)-1H-pyrazolo[3,4-d]pyrimidin-3-yl)phenyl)-1-

morpholinoethanone (**40e**) Yield =85.1%. ¹H NMR (400 MHz, DMSO-*d*₆) δ 8.30 (s, 1H), 7.69 (s, 2H), 7.60 (s, 2H), 7.48 (s, 2H), 7.35 (s, 2H), 6.72 (s, 2H), 5.51 (s, 2H), 3.83 (s, 2H), 3.54-3.48 (m, 8H); LC/MS (ESI, m/z) 430.19 [M + H]⁺.

1-(4-Aminophenyl)-3-(4-(4-methylpiperazin-1-yl)phenyl)-1H-pyrazolo[3,4-

d]pyrimidin-4-amine (**40f**) Yield =87.3%. ¹H NMR (400 MHz, DMSO-*d*₆) δ 8.28 (s, 1H), 7.61 (s, 2H), 7.50 (s, 2H), 7.19 (s, 2H), 7.04 (s, 2H), 6.70 (s, 2H), 5.40 (s, 2H), 3.84 (s, 2H), 3.26-3.12 (m, 6H), 2.78 (s, 3H); LC/MS (ESI, m/z) 401.22 [M + H]⁺.

1
2
3
4
5
6
7
8
9
10
11
12
13
14
15
16
17
18
19
20
21
22
23
24
25
26
27
28
29
30
31
32
33
34
35
36
37
38
39
40
41
42
43
44
45
46
47
48
49
50
51
52
53
54
55
56
57
58
59
60

1-(4-Aminophenyl)-3-(4-(4-ethylpiperazin-1-yl)phenyl)-1H-pyrazolo[3,4-d]pyrimidin-4-amine (40g) Yield =84.9%. ¹H NMR (400 MHz, DMSO-*d*₆) δ 8.28 (s, 1H), 7.68-7.61 (m, 4H), 7.16 (s, 2H), 6.70 (s, 2H), 5.32 (s, 2H), 3.76-3.43 (m, 4H), 2.93 (s, 4H), 2.51 (s, 2H), 1.21 (s, 3H); LC/MS (ESI, m/z) 415.23 [M + H]⁺.

1-(4-Aminophenyl)-3-(4-(1-ethylpiperidin-4-yl)phenyl)-1H-pyrazolo[3,4-d]pyrimidin-4-amine (40h) Yield =88.2%. ¹H NMR (400 MHz, DMSO-*d*₆) δ 8.31 (s, 1H), 7.69 (s, 4H), 7.44 (s, 2H), 6.70 (s, 2H), 5.31 (s, 2H), 3.17 (s, 4H), 2.66-2.56 (m, 2H), 2.25 (s, 2H), 1.85 (s, 4H), 1.10 (s, 3H); LC/MS (ESI, m/z) 415.23 [M + H]⁺.

Compound **41** was prepared following previously reported procedures.¹⁷

tert-butyl 4-(4-(4-amino-1-(4-aminophenyl)-1H-pyrazolo[3,4-d]pyrimidin-3-yl)phenyl)piperazine-1-carboxylate (42). Yield =86.7%. ¹H NMR (400 MHz, DMSO-*d*₆) δ 8.28 (s, 1H), 7.68 (s, 2H), 7.59 (s, 2H), 7.13 (s, 2H), 6.71 (s, 2H), 5.39 (s, 2H), 3.48 (s, 4H), 3.23 (s, 4H), 1.42 (s, 9H); LC/MS (ESI, m/z) 487.25 [M + H]⁺.

Antibodies and Chemicals. The following antibodies were purchased from Cell Signaling Technology (Danvers, MA): FLT3 (8F2) Rabbit mAb(#3462), Phospho-FLT3 (Tyr589/591) (30D4) Rabbit mAb(#3464), NF-κB p65 (D14E12) XP Rabbit mAb(#8242), Phospho-NF-κB p65 (Ser536) (93H1) Rabbit mAb(#3033), Stat5 Antibody(#9363), Phospho-Stat5 (Tyr694) (C71E5) Rabbit mAb(#9314), c-Myc (D84C12) XP Rabbit mAb(#5605), Akt (pan) (C67E7) Rabbit mAb(#4691), Phospho-Akt (Ser473) (D9E) XP Rabbit mAb(#4060), Phospho-Akt (Thr308) (244F9) Rabbit mAb(#4056), p44/42 MAPK (Erk1/2) (137F5) Rabbit mAb(#4695), Phospho-p44/42 MAPK (Erk1/2) (Thr202/Tyr204) (D13.14.4E) XP Rabbit mAb(#4370), GAPDH (D16H11) XP Rabbit mAb. Antibodies were used at 1:1000. Cells were lysed for 30 min

1
2
3 in lysis buffer supplemented with protease/phosphatase inhibitor cocktail (Cell Signaling
4 Technology). Lysates were cleared by centrifugation at 13,000 g at 4 °C for 10 min, and
5
6
7
8
9
10
11
12
13
14
15
16
17
18
19
20
21
22
23
24
25
26
27
28
29
30
31
32
33
34
35
36
37
38
39
40
41
42
43
44
45
46
47
48
49
50
51
52
53
54
55
56
57
58
59
60

in lysis buffer supplemented with protease/phosphatase inhibitor cocktail (Cell Signaling Technology). Lysates were cleared by centrifugation at 13,000 g at 4 °C for 10 min, and protein concentrations were determined by BCA. Lysates were subjected to electrophoresis through 10% or 15% gel and immobilized on the nitrocellulose membranes.

Compound **7** (AC220) was purchased from Shanghai Haoyuan Chemexpress Inc. (Shanghai, China).

TEL-Isogenic Cell Generation. Retroviral constructs for Ba/F3-TEL-FLT3 and Ba/F3-FLT3 mutants were made based on the pMSCVpuro (Clontech) backbone as described in the literature.²⁰ For TEL-fusion vectors, the first 1 kb of human TEL gene with an artificial myristoylation sequence (MGCGCSSHPEDD) was cloned into pMSCVpuro retroviral vector, followed by a 3xFLAG tag sequence and a stop codon. Then the kinase domain coding sequences of FLT3 variants were inserted in-frame between TEL and 3xFLAG sequences. For full-length expression vectors, the coding sequences of FLT3 variants were directly cloned in pMSCVpuro vector with a 3xFLAG tag at the C-terminal end. All mutations were performed using the QuikChange Site-Directed Mutagenesis Kit (Stratagene) following the manufacturer's instructions. Retrovirus was made using the same method described above and was used to infect Ba/F3 cells. After puromycin selection, the IL-3 concentration in the medium was gradually withdrawn until cells were able to grow in the absence of IL-3.

FLT3 wt/FLT3-ITD Protein Purification. The sequences of FLT3 wt and FLT3-ITD were amplified from the cDNA of HL60 and MV-4-11 cell lines. The cytoplasmic fragment 564-993 with His tag was cloned into baculovirus expression vector pFASTHT-

1
2
3 A. The recombinant bacmid was transfected into SF9 by Cellfectin (Invitrogen). High
4
5 titer viral stocks were obtained by two rounds of amplification of the virus. The protein
6
7 was expressed by infecting SF9 cells with high titer viral stocks for 48h. Cells were
8
9 harvested and re-suspended in lysis buffer (50 mM Tris pH 7.5, 150 mM NaCl, and 1
10
11 mM PMSF). The cells were lysed by ultra sonication and the cell debris was removed by
12
13 ultracentrifugation. The supernatant was incubated with Ni-affinity beads (GE). The
14
15 beads were then washed by lysis buffer containing 50-250mM imidazole. The elute was
16
17 loaded to superdex 75. The protein was concentrated to 1mg/ml and aliquots were frozen
18
19 and stored at -80 °C. The protein was used for ADP-Glo assay.
20
21
22
23

24
25 **Kinase Biochemical Assay.** The ADP-Glo kinase assay (Promega, Madison, WI)
26
27 was used to screen compd. **14** for its BTK, FLT3-WT, FLT3-ITD, FLT4, CDK11, CDK7,
28
29 CDK8, CSF1R, DDR1, DDR2, KIT, LCK, MKNK2, PDGFR α , PDGFR β and RET
30
31 inhibition effects, as well as compd. **7** for FLT3-WT and FLT3-ITD inhibition effects.
32
33 The kinase reaction system contains 4.95 μ L BTK (3 ng/ μ L), c-KIT (5 ng/ μ L), FLT3 (10
34
35 ng/ μ L), FLT3-ITD (10 ng/ μ L), PDGFR α (2.5 ng/ μ L), PDGFR β (1.25 ng/ μ L) and RET (5
36
37 ng/ μ L), 0.55 μ L of serially diluted drug and 5.5 μ L EGFR substrate poly (4:1 Glu, Tyr)
38
39 peptide (0.2 μ g/ μ L) (Promega, Madison, WI) with 40 μ M ATP (Promega, Madison, WI).
40
41 The reaction in each tube was started immediately by adding ATP and kept going for an
42
43 hour under 37 °C. After the tube was cooled for 5 minutes at room temperature, 5 μ L
44
45 solvent reactions were carried out in a 384-well plate. Then 5 μ L of ADP-Glo reagent
46
47 was added into each well to stop the reaction and consume the remaining ADP within 40
48
49 minutes. At the end, 10 μ L of kinase detection reagent was added into the well and
50
51 incubated for 30 minutes to produce a luminescence signal. Luminescence signal was
52
53
54
55
56
57
58
59
60

1
2
3 measured with an automated plate reader (Envision, PE, USA) and the dose-response
4
5 curve was fitted using Prism 5.0 (GraphPad Software Inc., San Diego, CA). The
6
7 biochemical tests of FLT4, CDK11, CDK7, CDK8, CSF1R, DDR1, DDR2, KIT, LCK,
8
9 MKNK2, PDGFR α , PDGFR β , and RET were provided by Invitrogen (Carlsbad, CA,
10
11 USA).

12
13
14
15 **Cell Culture and Proliferation Study.** The human AML cell lines MV4-11, U937
16
17 were purchased from the American Type Culture Collection (ATCC) (Manassas, VA,
18
19 USA). The FLT3-wt cell lines SKM-1, OCI-AML-2, HL-60, CMK were purchased from
20
21 Cobioer Biosciences CO., LTD (Nanjing, China). MOLM-13, MOLM14, and NB4 cell
22
23 lines were provided by Dr. Scott Armstrong, Dana Farber Cancer Institute (DFCI),
24
25 Boston, MA. MV4-11 was cultured in IMDM media (Corning, USA) with 10% FBS and
26
27 supplemented with 2% L-glutamine and 1% pen/strep. MOLM-13, MOLM-14, U937,
28
29 SKM-1, HL-60, CMK and FLT3 mutant isogenic BaF3 cells lines were cultured in RPMI
30
31 1640 media (Corning, USA) with 10% fetal bovine serum (FBS) and supplemented with
32
33 2% L-glutamine 1% penicillin/ streptomycin. OCI-AML-2 was cultured in α -MEM
34
35 media (Corning, USA) with 20% FBS and supplemented with 2% L-glutamine and 1%
36
37 pen/strep. All cell lines were maintained in culture media at 37 °C with 5% CO₂.
38
39
40
41
42

43
44 Cells were grown in 96-well culture plates (3000/well). The compounds of various
45
46 concentrations were added into the plates. Cell proliferation was determined after
47
48 treatment with compounds for 72 h. Cell viability was measured using the CellTiter-Glo
49
50 assay (Promega, USA) according to the manufacturer's instructions, and luminescence
51
52 was measured in a multilabel reader (Envision, PerkinElmer, USA). Data were
53
54 normalized to control groups (DMSO) and represented by the mean of three independent
55
56
57
58
59
60

1
2
3 measurements with standard error of < 20%. GI₅₀ values were calculated using Prism 5.0
4
5
6 (GraphPad Software, San Diego, CA).

7
8 **Signaling Pathway Study.** MOLM13, MOLM14, MV4-11 cells were treated with
9
10 DMSO, serially diluted compound **14**, 0.1 μM compound **7** (AC220) for 4 h. Cells were
11
12 then washed in PBS and lysed in cell lysis buffer. FLT3, Phospho-FLT3(Tyr589/591),
13
14 STAT5, Phospho-STAT5(Tyr694), AKT, Phospho-AKT Ser473, Phospho-AKT ERK,
15
16 Phospho44/42MAPK(Erk1/2) (Thr202/Tyr204), C-Myc, and GAPDH antibody (Cell
17
18 signaling Technology) were used for immunoblotting.
19
20

21
22 **Apoptosis Effect Examination.** MOLM13, MOLM14, MV4-11 cells were treated
23
24 with DMSO, serially diluted compound **14**, 0.1 μM compound **7** (AC220) for indicated
25
26 periods. Cells were then washed in PBS and lysed in cell lysis buffer. PARP, caspase-3,
27
28 GAPDH antibody (Cell Signaling Technology) were used for immunoblotting.
29
30

31
32 **Cell Cycle Analysis.** MOLM13, MOLM14, MV4-11 cells were treated with DMSO,
33
34 serially diluted compound **14**, 0.1 μM compound **7** (AC220) for indicated periods. The
35
36 cells were fixed in 70% cold ethanol and incubated at -20 °C overnight and then stained
37
38 with PI/RNase staining buffer (BD Pharmingen). Flow cytometry was performed using a
39
40 FACS Calibur (BD), and the results were analyzed by ModFit software.
41
42

43
44 **Modeling Method.** Currently there is no DFG-in conformation of FLT3 reported in
45
46 the PDB. It was obtained by homology modeling using the DFG-out conformation of
47
48 FLT3 (PDB ID: 4RT7) for the majority part and DFG-in conformation of CSF1R (PDB
49
50 ID: 3LCD) for the activation loop²¹ with Modeller 9.18²². The homology model was
51
52 further refined by MacroModel 11.5 (Schrödinger, LLC, New York, NY). For the DGF-
53
54 out conformation of FLT3, the PDB code 4XUF was prepared with Protein Preparation
55
56
57
58
59
60

1
2
3 Wizard (Schrödinger, LLC, New York, NY) for docking. The F691L mutation was
4
5 obtained by site mutation based on the optimized wild type coordinates. The ligands were
6
7 prepared with LigPrep (Schrödinger, LLC, New York, NY). The geometries were
8
9 optimized by Jaguar 9.5 (Schrödinger, LLC, New York, NY) at B3LYP/6-31G* level
10
11 with default settings. The atomic partial charges were calculated based on the optimized
12
13 ligand coordinates. The binding modes were obtained by Induced Fit (Schrödinger Suite
14
15 2017-1 Induced Fit Docking protocol) with extended sampling protocol. The best binding
16
17 modes were identified both by the IFD score and visual inspection of the binding
18
19 saturation to further reveal the binding mechanism.
20
21
22
23

24
25 **In Vivo Pharmacokinetics Study.** Compounds **14** and **7** was dissolved in 55% saline
26
27 containing 5% DMSO and 40% PEG400 by vortex. The final concentration of the stock
28
29 solution was 1 mg/mL for administration. Six 6–8 weeks old male Sprague-Dawely rats
30
31 were fasted overnight before starting drug treatment via intravenous and oral
32
33 administration. Animal blood collection time points were as follows: for intravenous
34
35 administration groups (I.V.), 1 min, 5 min, 15 min, 30 min, 1 h, 2 h, 4 h, 6 h, 8 h, 24 h
36
37 before and after administration were selected; for oral administration groups (P.O.), 5
38
39 min, 15 min, 30 min, 1 h, 2 h, 4 h, 6 h, 8 h, and 24 h before and after dosing were
40
41 selected. Each time about 0.2 mL of blood was collected through the jugular vein adding
42
43 heparin for anticoagulation and kept on ice. Then plasma was separated by centrifugation
44
45 at 8000 rpm for 6 min at 2–8 °C. The obtained plasma was stored at –80 °C before
46
47 analysis. After the test was finished, all surviving animals were transferred to the
48
49 repository or euthanaized (CO₂ asphyxiation).
50
51
52
53
54
55
56
57
58
59
60

1
2
3
4
5
6
7
8
9
10
11
12
13
14
15
16
17
18
19
20
21
22
23
24
25
26
27
28
29
30
31
32
33
34
35
36
37
38
39
40
41
42
43
44
45
46
47
48
49
50
51
52
53
54
55
56
57
58
59
60

MV4-11 Xenograft Tumor Model. Five-week-old female nu/nu mice were purchased from the Shanghai Experimental Center, Chinese Academy of Sciences (Shanghai, China). All animals were housed in a specific pathogen-free facility and used according to the animal care regulations of Hefei Institutes of Physical Science, Chinese Academy of Sciences (Hefei, China). Prior to implantation, cells were harvested during exponential growth. Five million MV4-11 cells in PBS were formulated as a 1:1 mixture with Matrigel (BD Biosciences) and injected into the subcutaneous space on the right flank of nu/nu mice. Daily oral administration was initiated when MV4-11 tumors had reached a size of 200–400 mm³. Animals were then randomized into treatment groups of 5 mice each for efficacy studies. Compound **14** was delivered daily in a HKI solution (0.5% methocellulose/0.4% Tween80 in ddH₂O) by oral gavage. A range of doses of compound **14** or its vehicle or compound **7** as control were administered, as indicated in the Figure 7 caption. Body weight was measured daily, and tumor growth was measured every other day after compound **14** treatment. Tumor volume was calculated as follows: tumor volume (mm³) = [(W² × L)/2] in which width (W) is defined as the smaller of the two measurements and length (L) is defined as the larger of the two measurements.

HE Staining. HE staining was carried out according to previous publication.²³ First, the sections were hydrated and then the slide was dipped into a Coplin jar containing Mayer's hematoxylin and agitated for 30 s. After rinsing the slide in H₂O for 1 min, it was stained with 1% eosin Y solution for 10–30 s with agitation. Subsequently, the sections were dehydrated with two changes of 95% alcohol and two changes of 100% alcohol for 30 s each, and then the alcohol was extracted with two changes of xylene. Finally, one or two drops of mounting medium was added and covered with a coverslip.

1
2
3
4
5
6
7
8
9
10
11
12
13
14
15
16
17
18
19
20
21
22
23
24
25
26
27
28
29
30
31
32
33
34
35
36
37
38
39
40
41
42
43
44
45
46
47
48
49
50
51
52
53
54
55
56
57
58
59
60

K_i-67 Staining. For IHC demonstration of K_i-67, tissue sections were quenched for endogenous peroxides and placed in an antigen retrieval solution (0.01 M citrate buffer, PH 6.0) for 15 min in a microwave oven at 100 °C at 600 W. After incubation in the casein block, mouse mAb anti-K_i-67 (ZSGB-BIO, China) was applied to the sections at dilutions of 1:50. Incubations with primary antibodies lasted overnight at 4 °C. The secondary detection system was used to visualize antibody binding. Staining was developed with DAB, and the slides were counterstained with hematoxylin, dehydrated and mounted.

TUNEL Staining. TUNEL staining was performed using the POD in situ cell death detection kit (Roche, USA). Briefly, sections were deparaffinized in xylene, rehydrated in decreasing concentration of ethanol, and then treated by nuclease free proteinase K for 15 min at room temperature before endogenous peroxidase was blocked in 3% H₂O₂ in methanol. Terminal deoxynucleotidyl transferase (TdT) in reaction buffer was applied to sections for 1 h at 37 °C. Following washes, the slides were covered by converter-POD solution for 30 min at 37 °C. Apoptotic cells were detected after incubation in 3,3'-diaminobenzidine (DAB) chromogen (Beyotime Biotechnology, China) for approximately 8 min, and the slides were counterstained with hematoxylin.

ASSOCIATED CONTENT

Supporting Information

The supporting information is available free of charge on the ACS Publication website at <http://pubs.acs.org>.

Table S1 listing the DiscoverX's KinomeScan selectivity profiling data of compound **14**.

1
2
3 Figure S1 showing the cellular effects of compound 7 in FLT3-ITD positive AML cell
4
5 line.
6

7
8 Molecular formula strings (CSV)
9

10 **AUTHOR INFORMATION**

11 **Corresponding Authors**

12
13
14
15
16 * For R.X: phone: 86-551-62923145; Email: xrx2041@163.com.

17
18 *For J.L.: phone: 86-551-65593186; E-mail: jingliu@hmfl.ac.cn.

19
20
21 *For Q.L.: phone: 86-551-65595161; E-mail: qsliu97@hmfl.ac.cn.
22
23

24 **Author Contributions**

25
26
27 The manuscript was written through contributions of all authors. All authors have given
28 approval to the final version of the manuscript. A.W., X.L., C.C., H.W., Z.Q. and C.H.
29 contributed equally to this work.
30
31
32

33 **Notes**

34
35
36
37 Dr. Shanchun Zhang is a shareholder of Hefei Cosource Medicine Technology Co. LTD.
38
39
40

41 **ACKNOWLEDGMENTS**

42
43
44 This work was supported by the National Natural Science Foundation of China (nos.
45 U1432250, U1532154, 81471773, 81473088), the National Key Research and
46 Development Program of China (no. 2016YFA0400900), the “Personalized Medicines-
47 Molecular Signature-Based Drug Discovery and Development”, Strategic Priority
48 Research Program of the Chinese Academy of Sciences (no. XDA12020308), the Natural
49 Science Foundation of Anhui province (nos. 1608085QH180, 1708085MH208), the
50
51
52
53
54
55
56
57
58
59
60

1
2
3 Postdoctoral Innovative Talents Support Program (no. BX201600169) and the
4 CAS/SAFEA international partnership program for creative research teams. We are also
5 grateful for the National Program for Support of Top-Notch Young Professionals for J.L.
6 and the “Hundred Talents Program” of CAS support for J.L. and W.W..
7
8
9
10
11

12 13 14 **ABBREVIATIONS USED**

15
16 AML, Acute myeloid leukemia; FLT3, Fms-like tyrosine kinase 3; RTK, receptor
17 tyrosine kinase; FLT3-ITD, FMS-like tyrosine kinase internal tandem duplication; BTK,
18 Bruton's tyrosine kinase; CLL, chronic lymphocytic leukemia; MCL, mantle cell
19 lymphoma; SAR, structure-activity relationship; DMSO, dimethylsulfoxide; DMF, *N,N*-
20 dimethylformamide; DCM, dimethylchloride; TUNEL, terminal deoxynucleotidyl
21 transferase dUTP nick end labeling.
22
23
24
25
26
27
28
29
30

31 32 **REFERENCES**

- 33
34 (1) Lee, H. K.; Kim, H. W.; Lee, I. Y.; Lee, J.; Lee, J.; Jung, D. S.; Lee, S. Y.; Park, S. H.;
35 Hwang, H.; Choi, J. S.; Kim, J. H.; Kim, S. W.; Kim, J. K.; Cools, J.; Koh, J. S.; Song, H.
36 J. G-749, a novel FLT3 kinase inhibitor, can overcome drug resistance for the treatment
37 of acute myeloid leukemia. *Blood* **2014**, 123, 2209-2219.
38
39 (2) Kiyoi, H. FLT3 Inhibitors: recent advances and problems for clinical application.
40 *Nagoya J. Med. Sci.* **2015**, 77, 7-17.
41
42 (3) Fathi, A. T.; Chen, Y. B. The role of FLT3 inhibitors in the treatment of FLT3-mutated
43 acute myeloid leukemia. *Eur. J. Haematol.* **2017**, 98, 330-336.
44
45 (4) Smith, C. C.; Lin, K.; Stecula, A.; Sali, A.; Shah, N. P. FLT3 D835 mutations confer
46 differential resistance to type II FLT3 inhibitors. *Leukemia* **2015**, 29, 2390-2392.
47
48 (5) Weisberg, E.; Roesel, J.; Furet, P.; Bold, G.; Imbach, P.; Florsheimer, A.; Caravatti,
49
50
51
52
53
54
55
56
57
58
59
60

1
2
3 G.; Jiang, J.; Manley, P.; Ray, A.; Griffin, J. D. Antileukemic effects of novel first- and
4 second-Generation FLT3 Inhibitors: structure-affinity comparison. *Genes Cancer* **2010**,
5
6 1, 1021-1032.
7
8

9
10 (6) Zhao, Z.; Wu, H.; Wang, L.; Liu, Y.; Knapp, S.; Liu, Q.; Gray, N. S. Exploration of
11 type II binding mode: a privileged approach for kinase inhibitor focused drug discovery?
12
13 *ACS Chem. Biol.* **2014**, 9, 1230-1241.
14
15

16
17 (7) Yee, K. W.; Schittenhelm, M.; O'Farrell, A. M.; Town, A. R.; McGreevey, L.;
18 Bainbridge, T.; Cherrington, J. M.; Heinrich, M. C. Synergistic effect of SU11248 with
19 cytarabine or daunorubicin on FLT3 ITD-positive leukemic cells. *Blood* **2004**, 104, 4202-
20 4209.
21
22

23
24 (8) Lee, L. Y.; Hernandez, D.; Rajkhowa, T.; Smith, S. C.; Raman, J. R.; Nguyen, B.;
25 Small, D.; Levis, M. Preclinical studies of gilteritinib, a next-generation FLT3 inhibitor.
26
27 *Blood* **2017**, 129, 257-260.
28
29

30
31 (9) Smith, C. C.; Lasater, E. A.; Lin, K. C.; Wang, Q.; McCreery, M. Q.; Stewart, W. K.;
32 Damon, L. E.; Perl, A. E.; Jeschke, G. R.; Sugita, M.; Carroll, M.; Kogan, S. C.; Kuriyan,
33 J.; Shah, N. P. Crenolanib is a selective type I pan-FLT3 inhibitor. *Proc. Natl. Acad. Sci U.*
34
35 *S. A.* **2014**, 111, 5319-5124.
36
37

38
39 (10) Weisberg, E.; Boulton, C.; Kelly, L. M.; Manley, P.; Fabbro, D.; Meyer, T.; Gilliland,
40 D. G.; Griffin, J. D. Inhibition of mutant FLT3 receptors in leukemia cells by the small
41
42 molecule tyrosine kinase inhibitor PKC412. *Cancer Cell* **2002**, 1, 433-443.
43
44

45
46 (11) Smith, C. C.; Zhang, C.; Lin, K. C.; Lasater, E. A.; Zhang, Y.; Massi, E.; Damon, L.
47
48 E.; Pendleton, M.; Bashir, A.; Sebra, R.; Perl, A.; Kasarskis, A.; Shellooe, R.; Tsang, G.;
49
50 Carias, H.; Powell, B.; Burton, E. A.; Matusow, B.; Zhang, J.; Spevak, W.; Ibrahim, P. N.;
51
52
53
54
55
56
57
58
59
60

1
2
3
4
5
6
7
8
9
10
11
12
13
14
15
16
17
18
19
20
21
22
23
24
25
26
27
28
29
30
31
32
33
34
35
36
37
38
39
40
41
42
43
44
45
46
47
48
49
50
51
52
53
54
55
56
57
58
59
60

Le, M. H.; Hsu, H. H.; Habets, G.; West, B. L.; Bollag, G.; Shah, N. P. Characterizing and overriding the structural mechanism of the quizartinib-resistant FLT3 "gatekeeper" F691L mutation with PLX3397. *Cancer Discovery* **2015**, *5*, 668-679.

(12) Shah, N. P.; Talpaz, M.; Deininger, M. W.; Mauro, M. J.; Flinn, I. W.; Bixby, D.; Lustgarten, S.; Gozgit, J. M.; Clackson, T.; Turner, C. D.; Haluska, F. G.; Kantarjian, H.; Cortes, J. E. Ponatinib in patients with refractory acute myeloid leukaemia: findings from a phase 1 study. *Br. J. Hematol.* **2013**, *162*, 548-552.

(13) Zarrinkar, P. P.; Gunawardane, R. N.; Cramer, M. D.; Gardner, M. F.; Brigham, D.; Belli, B.; Karaman, M. W.; Pratz, K. W.; Pallares, G.; Chao, Q.; Sprankle, K. G.; Patel, H. K.; Levis, M.; Armstrong, R. C.; James, J.; Bhagwat, S. S. AC220 is a uniquely potent and selective inhibitor of FLT3 for the treatment of acute myeloid leukemia (AML). *Blood* **2009**, *114*, 2984-2992.

(14) Man, C. H.; Fung, T. K.; Ho, C.; Han, H. H.; Chow, H. C.; Ma, A. C.; Choi, W. W.; Lok, S.; Cheung, A. M.; Eaves, C.; Kwong, Y. L.; Leung, A. Y. Sorafenib treatment of FLT3-ITD(+) acute myeloid leukemia: favorable initial outcome and mechanisms of subsequent nonresponsiveness associated with the emergence of a D835 mutation. *Blood* **2012**, *119*, 5133-5143.

(15) Herrera, A. F.; Jacobsen, E. D. Ibrutinib for the treatment of mantle cell lymphoma. *Clin. Cancer Res.* **2014**, *20*, 5365-5371.

(16) Brown, J. R. Ibrutinib (PCI-32765), the first BTK (Bruton's tyrosine kinase) inhibitor in clinical trials. *Curr. Hematol. Malig. Rep.* **2013**, *8*, 1-6.

(17) Wu, H.; Hu, C.; Wang, A.; Weisberg, E. L.; Wang, W.; Chen, C.; Zhao, Z.; Yu, K.; Liu, J.; Wu, J.; Nonami, A.; Wang, L.; Wang, B.; Stone, R. M.; Liu, S.; Griffin, J. D.; Liu,

1
2
3 J.; Liu, Q. Ibrutinib selectively targets FLT3-ITD in mutant FLT3-positive AML.
4
5 *Leukemia* **2016**, 30, 754-757.

6
7
8 (18) Li, X.; Wang, A.; Yu, K.; Qi, Z.; Chen, C.; Wang, W.; Hu, C.; Wu, H.; Wu, J.; Zhao,
9
10 Z.; Liu, J.; Zou, F.; Wang, L.; Wang, B.; Wang, W.; Zhang, S.; Liu, J.; Liu, Q. Discovery
11
12 of (R)-1-(3-(4-Amino-3-(4-phenoxyphenyl)-1H-pyrazolo[3,4-d]pyrimidin-1-yl)piperidin-
13
14 1-yl)-2-(dimethylamino)ethanone (CHMFL-FLT3-122) as a potent and orally available
15
16 FLT3 Kinase inhibitor for FLT3-ITD positive acute myeloid leukemia. *J. Med. Chem.*
17
18 **2015**, 58, 9625-9638.

19
20
21 (19) Zorn, J. A.; Wang, Q.; Fujimura, E.; Barros, T.; Kuriyan, J. Crystal structure of the
22
23 FLT3 kinase domain bound to the inhibitor quizartinib (AC220). *PLoS One* **2015**, 10,
24
25 e0121177.

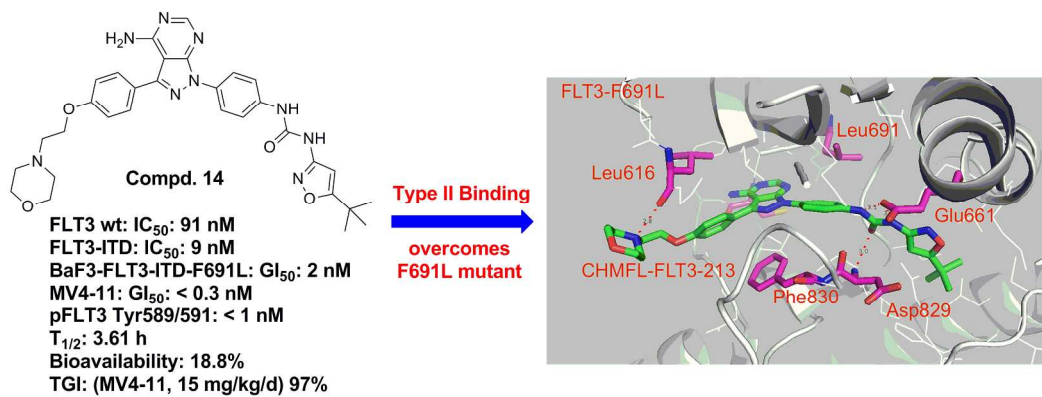
26
27
28 (20) Davis, M. I.; Hunt, J. P.; Herrgard, S.; Ciceri, P.; Wodicka, L. M.; Pallares, G.;
29
30 Hocker, M.; Treiber, D. K.; Zarrinkar, P. P. Comprehensive analysis of kinase inhibitor
31
32 selectivity. *Nat. Biotechnol.* **2011**, 29, 1046-1051.

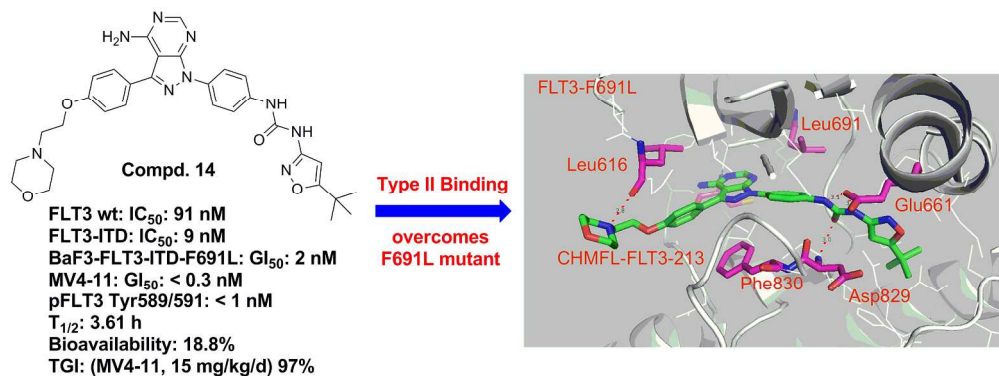
33
34
35 (21) Ke, Y. Y.; Singh, V. K.; Coumar, M. S.; Hsu, Y. C.; Wang, W. C.; Song, J. S.; Chen,
36
37 C. H.; Lin, W. H.; Wu, S. H.; Hsu, J. T.; Shih, C.; Hsieh, H. P. Homology modeling of
38
39 DFG-in FMS-like tyrosine kinase 3 (FLT3) and structure-based virtual screening for
40
41 inhibitor identification. *Sci. Rep.* **2015**, 5, 11702.

42
43
44 (22) Sali, A.; Blundell, T. L. Comparative protein modelling by satisfaction of spatial
45
46 restraints. *J. Mol. Biol.* **1993**, 234, 779-815.

47
48
49 (23) Pollard, J. W. Trophic macrophages in development and disease. *Nat. Rev. Immunol.*
50
51 **2009**, 9, 259-270.

Table of Contents Graphic





230x85mm (300 x 300 DPI)